Probing Long-Range Polymer Chain Dynamics of Poly(*L*-lysine) in Aqueous Solution by Fluorescence

by

Hummara Aslam

A thesis
presented to the University of Waterloo
in fulfillment of the
thesis requirement for the degree of
Master of Science
in
Chemistry

Waterloo, Ontario, Canada, 2011

I hereby declare that I am the sole author of this thesis. This is a true copy of the thesis, including any required final revisions, as accepted by my examiners.

I understand that my thesis may be made electronically available to the public.

Abstract

Information about long-range polymer chain dynamics (LRPCD) can be obtained by attaching a luminophore and its quencher onto a polymer and monitoring the rate at which the luminophore is quenched. Since a quenching event represents an encounter between the luminophore and the quencher, the rate of quenching reflects the dynamics undergone by those polymer segments bearing the fluorescent probes. Following a long tradition, pyrene is considered to be the luminophore of choice for conducting these experiments due to pyrene's ability to form an excimer upon encounter between an excited pyrene and a ground-state pyrene. In effect, pyrene acts as both the luminophore and the quencher. Unfortunately, pyrene is highly hydrophobic, which prevents its use to probe the chain dynamics of water-soluble polymers. This study is an attempt at circumventing the problems associated with the hydrophobicity of pyrene by covalently labeling a water-soluble poly(*L*-lysine) (PLL) with a ruthenium complex and dinitrobenzene to act as water-soluble luminophore and quencher, respectively.

A phenanthroline derivative of the ruthenium bipyridyl complex $Ru(bpy)_3^{2+}$, namely ruthenium (II) bisbipyridine 5-aminophenanthroline chloride ($RuNH_2$), was synthesized to use as a luminophore. Phenanthroline is a ligand bearing a reactive amine, which after modification into an isothiocyanate allows the attachment of the ruthenium complex (RuNCS) onto PLL. The two positive charges of ruthenium enhance the solubility of the luminophore in aqueous solution. In addition, the observed lifetime of $RuNH_2$ at 20 °C is ~0.6 μsec which provides a long enough time window to probe the LRPCD of PLL.

PLL was randomly labeled with the luminophore, RuNCS, and a quencher, 1-fluoro-2,4-dinitrobenzene (FDNB) to yield Ru-PLL-Q. The Ru-PLL-Q samples were characterized and the labeling level of the different Ru-PLL-Q samples was determined. Next, aqueous solutions of the Ru-PLL-Q samples were prepared at different pH's, their time-resolved fluorescence decays were acquired and analyzed with the Fluorescence Blob Model (FBM) that accounts for the random distribution of the labels along the chain. The fluorescence quenching experiments yield a measure of the internal dynamics of PLL which appear to slow down when the pH is increased from 3 to values larger than 5. Slower internal dynamics at higher pH's are expected since PLL adopts an α-helical conformation, as evidenced by circular dichroism experiments. Molecular mechanics optimizations suggest that the distance over which quenching of the Ru complex occurs is compatible with the geometry of the PLL construct. These preliminary results suggest that a ruthenium complex and dinitrobenzene have the potential to offer an attractive alternative to the use of pyrene to study the chain dynamics of water-soluble polymers quantitatively.

Acknowledgements

I want to thank my supervisor Jean Duhamel foremost, not only for his support, guidance and encouragement for this project but also for always being a source of inspiration for me. I've come a long way and it wouldn't have been possible without his great help.

I would also like to thank my husband for his support, kindness and love despite the distance.

I have to thank my big list of friends. They all mean a lot to me and I am truly blessed to have them in my life.

Special thanks go to my current and former lab colleagues for all their help and guidance. It was wonderful working them.

Finally, I want to acknowledge my family especially my parents and sisters, for all they have done for me. I can't thank my brother enough for believing in me and always being there for me. And, last but not least, my nephews and nieces who can always manage to bring a smile on my face are also appreciated. I love you all!

And, obviously none of this work would have been possible without the great help from God almighty; I am very thankful to Him.

Table of Contents

LIST OF FIGURES……..vii

LIST OF SCHEMES……ix

LIST OF ABBREVIATIONS ……...x

LIST OF SYMOLS……xi

1. INTRODUCTION **1**

1.1. LONG RANGE POLYMER CHAIN DYNAMICS **1**
1.2. END LABELING VERSUS RANDOM LABELING **2**
1.3. FLUORESCENCE BLOB MODEL (FBM) **4**
1.4. THE LUMINOPHORE :RUTHENIUM BIPYRIDYL COMPLEX **5**
1.5. THE QUENCHER: 1-FLUORO-2,4-DINITROBENZENE **7**
1.6. POLYMER FOR THE PROJECT: POLY(*L*-LYSINE) **8**
1.7. OBJECTIVE OF THE PROJECT **12**

2. EXPERIMENTAL **13**

2.1. MATERIALS **13**
2.2. INSTRUMENTATION **13**
2.3. SYNTHESIS PROCEDURES **15**
2.3.1. SYNTHESIS OF THE WATER-SOLUBLE DYE……... **15**
2.3.2. PLL LABELING……..**18**
2.3.3. RU AND DINITROBENZENE CONTENT DETERMINATION…….. **22**
2.4. ANALYSIS **28**

3. RESULTS AND DICUSSION **30**

3.1. CHARACTERIZATION OF THE PRODUCTS **30**
3.2. FBM ANALYSIS OF TIME-RESOLVED FLUORESCENCE DECAYS **39**
3.3. CIRCULAR DICHROISM **45**
3.4. SUMMARY OF EXPERIMENTAL RESULTS OBTAINED BY FLUORESCENCE… **47**

3.5. MOLECULAR MECHANICS OPTIMIZATIONS…….**49**

4. CONCLUSIONS AND FUTURE WORK **60**

4.1. CONCLUSIONS **60**
4.2. FUTURE WORK **63**

REFERENCES **65**

APPENDIX A **68**

List of Figures

Figure 1.1. Illustration of the Fluorescence Blob Model. **4**

Figure 1.2. Structure of ruthenium trisbipyridine $Ru(bpy)_3^{2+}$.....**6**

Figure 1.3. Absorption spectrum of $Ru(bpy)_3^{2+}$ Cl_2^{-1} in a 0.1 M Na_2CO_3 solution (pH 9.6)……...**7**

Figure 1.4. Structure of 1-fluoro-2,4-dinitrobenzene (FDNB). **8**

Figure 1.5. Structure of Poly (*L*-lysine) (PLL). **9**

Figure 1.6. CD spectra of PLL under different conditions. **11**

Figure 2.1. Absorption spectrum for (A) $Ru(bpy)_2Cl_2$, (B) 5-amino-1,10-phenanthroline, and (C) $RuNH_2$ in DMF…….**16**

Figure 2.2. Structure of PLL randomly labeled with the chromophore and quencher.....**19**

Figure 2.3. Normalized absorption spectra of Ru-PLL (——) and PLL-Q (·····) obtained in milli-Q water.....**23**

Figure 3.1. Absorption and emission (λ_{ex}= 454 nm) spectra of 20 μM $RuNH_2$ in 0.1 M Na_2CO_3 at pH 9.6......**30**

Figure 3.2. Fluorescence decay for $RuNH_2$ in degassed 0.1 M Na_2CO_3 solution at pH 9.6; λ_{ex}= 454 nm and λ_{em}= 610 nm……**31**

Figure 3.3. Absorption and emission spectra (λ_{ex}= 454 nm) of $Ru_{2.6}$-PLL in a 0.1 M Na_2CO_3 at pH 9.6 [$Ru_{2.6}$-PLL = 20μM].....**32**

Figure 3.4. Fluorescence decay for $Ru_{2.6}$-PLL in a degassed aqueous solution (λ_{ex}= 454 nm and λ_{em}= 610 nm). **33**

Figure 3.5. Absorption spectra of 15 μM $Ru_{2.6}$-PLL (…….) and 20 μM $Ru_{2.5}$-PLL-Q_{11} (- - - -) in milli-Q water. **36**

Figure 3.6. Fluorescence decays of a) $Ru_{2.6}$-PLL and b) $Ru_{2.5}$-PLL-Q_{11} in a degassed aqueous solution (λ_{ex}= 454 nm and λ_{em}= 610 nm). **37**

Figure 3.7. Plot of the ratio Q of $<\tau>_N$ of Ru-PLL over $<\tau>_N$ of Ru-PLL-Q against the quencher content. **38**

Figure 3.8. Fluorescence decay for Ru-PLL-Q sample in a degassed aqueous solution (λ_{ex}= 454 nm, λ_{em}= 610 nm, χ^2=1.1).....**39**

Figure 3.9. Plots of a) N_{blob}, b) k_{blob} c) $k_{blob} \times N_{blob}$ against the corrected quencher content (λ_Q/f_{diff})……**41**

Figure 3.10. Plots of a) N_{blob}, b) k_{blob}, and c) $N_{blob} \times k_{blob}$ against the corrected quencher content (λ_Q/f_{diff}) for pH 13 (□), pH 11 (△), pH 9 (●), pH 7 (▲), pH 5 (■), pH 3 (×). **43**

Figure 3.11. Circular dichroism spectra for a) PLL, and b) Ru-PLL-Q samples in milli-Q water for pH 3 (·····), pH 5 (--------), pH 7 (- - - -), pH 9 (- ·· - ·· -), pH 11 (——), and pH 13 (———).....…**46**

Figure 3.12. Plot of $N^0{}_{blob}$ and $(k_{blob} \times N_{blob})^0$ a function of pH for Ru-PLL-Q samples….

…….....**48**

Figure 3.13. A) A Ru-PLL-Q construct bearing the Ru complex and DNB at the 8th and 9th residue, respectively, and B) the Ru complex and DNB are located at the 8th and 31st residue, respectively.....……**50**

Figure 3.14. Distance of closest approach, $d_{Ru\text{-}DNB}$, as a function of the number of lysine residues, N_{Lys}, between the Ru complex attached on the 8th residue and DNB attached at positions 9 to 35 along a PLL α-helix.....**51**

Figure 3.15. $<\tau>_N^o / <\tau>_N$ as a function of dinitrobenzene concentration in 0.01 M NaCl aqueous solution a) $RuNH_2$ b) 1-pyrenemethanol.....**53**

Figure 3.16. a) A construct of $(Gly)_8$-$(Lys\text{-}Ru)_1$-$(Gly)_1$-$(Glu\text{-}PMA)_1$-$(Gly)_8$, b) A construct of $(Gly)_8$-$(Lys\text{-}Ru)_1$-$(Gly)_1$-($Glu\text{-}PBA)_1$-$(Gly)_8$. **55**

Figure 3.17. An α-helical construct of $(Gly)_8$-$(Lys\text{-}DNB)_1$-$(Gly)_8$.....**56**

Figure 3.18. Determination of V_{blob} using the Equation 4.2B for a) PGA-PBA and Ru-PLL-Q chains by assuming b) r = 15Å, and c) r = 11Å. **58**

List of Schemes

Scheme 1.1. Synthesis of $RuNH_2$ **2**

Scheme 2.1. Synthesis of RuNCS. **15**

Scheme 2.1. Labeling of PLL with RuNCS to yield Ru-PLL. **17**

Scheme 2.3. Labeling of Ru-PLL with FDNB to yield Ru-PLL-Q. **20**

List of Abbreviations

^{1}H NMR	Proton Nuclear Magnetic Resonance
CD	Circular Dichroism
EEC	End-to-End Cyclization
ESR	Electron Spin Resonance
FBM	Fluorescence Blob Model
FDNB	1-Fluoro-2,4-Dinitrobenzene
FDQ	Fluorescence Dynamic Quenching
LRPCD	Long Range Polymer Chain Dynamics
MLCT	Metal-to-Ligand Charge Transfer
MS	Mass Spectrometry
PDI	Polydispersity Index
PDMA	Poly(*N*, *N*-dimethylacrylamide)
PGA	Poly(*L*-Glutamic Acid)
PLL	Poly(*L*-lysine)
$Ru(bpy)_3^{2+}$	Ruthenium (II) Trisbipyridine
RuNCS	Bis-(2,2-Bipyridine)-Ruthenium (II)-5-Isothiocyanato-1,10-Phenanthroline Chloride
$RuNH_2$	Bis-(2,2-Bipyridine)-Ruthenium (II)-5-Amino-1,10-Phenanthroline Chloride
Ru-PLL	RuNCS labeled PLL
Ru-PLL-Q	PLL labeled with RuNCS and DNB
SPC	Single Photon Counting
UV	Ultraviolet-Visible

List of Symbols

[θ]	Molar ellipiticity
f_α	Alpha-helical content
λ_Q	Quencher content per gram of polypeptide
λ_{Ru}	Ruthenium content per gram of polypeptide
x_Q	Molar fraction of lysines labeled with Q
x_{Ru}	Molar fraction of lysines labeled with Ru

1. Introduction

1.1. Long range polymer chain dynamics

The internal dynamics of polymers affect their behavior in solution, such as during the folding of a protein along a given folding pathway[1] or the shear thinning of an associative polymer solution.[2] The time scale over which chain dynamics manifest themselves can be probed by monitoring how polymer motions induce the loss of orientation of a monomer in the chain or enable two well-separated monomers to encounter. The experiments probing the loss of orientation of a monomer include Electron Spin Resonance (ESR),[3] Nuclear Magnetic Resonance (NMR),[4] and Fluorescence Anisotropy (FA).[5] These techniques monitor the local chain dynamics that affect a backbone segment made of just a few monomers, typically 3 to 5.[6] On the other hand, long-range polymer chain dynamics (LRPCD) can be probed by attaching a luminophore and quencher at the ends of a polymer and measuring their rate of encounter by fluorescence in a Fluorescence Dynamic Quenching (FDQ)[7-9] experiment.

In a typical FDQ experiment, a monodisperse polymer chain is labeled with a quencher (Q) and luminophore (D) at both ends.[7,8] Upon absorption of a photon, the luminophore can either emit fluorescence with a lifetime τ_D, or encounter the quencher with a rate constant k_{cy}.[7,8] This process is described in Scheme 1.1.

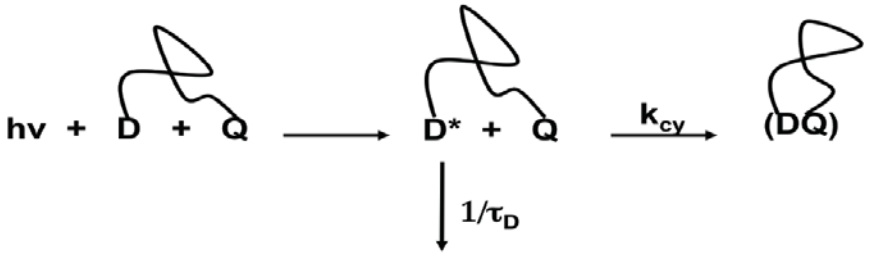

Scheme 1.1. Kinetic scheme describing the encounter between a luminophore (D) and quencher (Q) attached to the ends of a polymer chain.[7,8]

A common luminophore used for FDQ experiments is pyrene.[7] Pyrene presents the advantage that it can act both as a quencher and a luminophore. A pyrene monomer in the excited state can encounter another pyrene monomer in the ground-state, giving rise to an excimer. In effect, excimer formation quenches the excited pyrene monomer. Thus, using pyrene simplifies the labeling procedure, as only one labeling step is required instead of the two needed when both the luminophore and quencher have to be covalently attached to the polymer.

1.2. End Versus Random Labeling of a Polymer

As mentioned earlier the well-accepted strategy employed to study LRPCD by FDQ experiments involves the covalent attachment of a pyrenyl derivative to the ends of a monodisperse polymer chain and monitoring the process of excimer formation of these two pyrenyl moities in a process known as end-to-end cyclization (EEC). EEC is described by a single rate constant, k_{cy}, which gives information on the dynamics of the polymer backbone in solution.[7,10] Although EEC has been used extensively and gives valuable information about polymer chain dynamics, it has many drawbacks. Firstly, the synthesis of end labeled

polymers is complicated because both chain ends should have functional groups to allow the attachment of pyrene. Secondly, only monodisperse polymer chains can be used if the EEC kinetics are to be described by a single rate constant. Thirdly, since the polymer chain is probed solely through the interactions of the labeled ends, the bulk of the chain becomes invisible and information about the chain ends only is retrieved. Fourthly, k_{cy} depends strongly on the polymer chain length (N). In practice, k_{cy} takes values that are large enough to be determined experimentally only for short and flexible polymer chains. Therefore, EEC experiments are usually not used to study the LRPCD of polymers containing more than 100 monomers.[11]

This situation is somewhat unfortunate because long chains are usually more representative of the properties of a polymer. If too long a chain maintains the luminophore and quencher too far apart, a simple solution would be to bring the luminophore and the quencher closer to each other by randomly labeling the polymer chain with the luminophore and its quencher. However, the encounters between luminophores and quenchers randomly distributed along a polymer chain are described by a distribution of rate constants that complicates the analysis of fluorescence data. This distribution of rate constants results from the strong dependence of k_{cy} on the length of the polymer segment spanning a luminophore and a quencher.[12] Thus, a new model is required to analyze the decays obtained from a randomly labeled polymer chain.

1.3. Fluorescence Blob Model (FBM)

In 1999, the Duhamel laboratory proposed a mathematical model known as the Fluorescence Blob Model (FBM) to study the complicated decays associated with the random labeling of a polymer chain.[12] The FBM arbitrarily divides the coil of a randomly labeled polymer chain into blobs, where a blob is the volume of the polymer coil being probed by the excited luminophore during its lifetime. This arbitrary division of a polymer coil into a cluster of blobs of volume V_{blob} is depicted in Figure 1.1. The rate constant for diffusional encounter between an excited luminophore and a quencher located inside a same blob is given by k_{blob}. The local concentration of blobs inside a polymer coil is given by [*blob*] and the number of structural units of the polymer coil per blob is N_{blob}.[12,13]

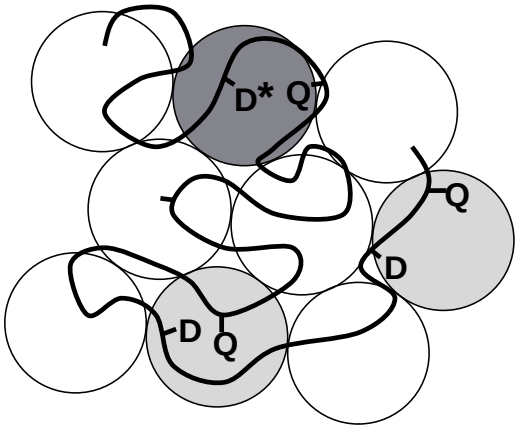

Figure 1.1. Illustration of the Fluorescence Blob Model where the solid line, D, and Q represent the polymer coil, luminophore, and quencher, respectively. Dark grey, light grey, and white circles represent blobs containing an excited luminophore and quencher, a ground-state luminophore and quencher, and no luminophore or quencher, respectively.

The first polymer analyzed with the FBM was pyrene-labeled polystyrene (PS).[12] Since then, it has been applied to several other polymers such as pyrene-labeled poly(*N*,*N*-dimethylacrylamide) (PDMA)[14] and polyisoprene (PI)[15] to study LRPCD in organic solvents, pyrene-labeled poly(*L*-glutamic acid) (PGA) to study side-chain dynamics in organic solvents,[16,17] and several pyrene-labeled hydrophobically modified water-soluble polymers to study the hydrophobic association of the pyrene labels in aqueous solutions.[18,19] These studies used the FBM as an analytical tool to describe the internal dynamics of polymers, either the LRPCD for PS, PDMA, and PI, or short-range side-chain dynamics for PGA. However, all of these studies were carried out in organic solvents to solubilize the hydrophobic pyrene labels.

The present project represents the first attempt to apply the FBM to study the LRPCD of a polymer in aqueous solution. Pyrene would have been the luminophore of choice for such a study were it not for its hydrophobicity. To address this problem, a water-soluble luminophore was used to label the polymer together with a suitable water-soluble quencher to investigate the LRPCD of the polymer in aqueous solution.

1.4. The Luminophore: Ruthenium Bipyridyl Complex

Luminescent transition metal complexes with polypyridyl bridging ligands such as 2,2'-bipyridyl, 4,4'-bipyridyl, and 1,10-phenanthroline have shown considerable promise and are receiving increasing attention because of their unique photophysical and redox properties.[19] Especially, ruthenium (II) polypyridyl complexes are being used in numerous applications such as light emitting devices,[19] DNA probes,[20] and fiber optic sensors[21]

because of their relatively long-lived excited states, rich redox chemistry, and thermal and photochemical stability.

The best known ruthenium bipyridyl complex, ruthenium (II) trisbipyridine ($Ru(bpy)_3^{2+}$), is shown in Figure 1.2. $Ru(bpy)_3^{2+}$ is a metal complex whose chemical composition can be represented as a MX_6d^6 metal complex where M is the metal and X is a ligand that binds at one site.[23] The complexation of three identical ligands with Ru^{2+} gives this complex a high level of symmetry. Ru^{2+} is a d^6 transition metal and the polypyridine ligands are usually colorless molecules containing σ donor orbitals localized on the nitrogen atoms and π donor and π* acceptor orbitals more or less delocalized on the aromatic rings.[19]

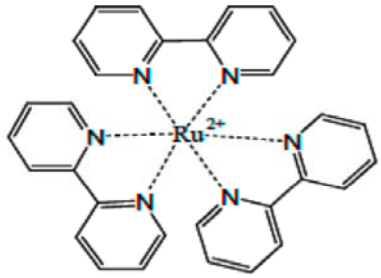

Figure 1.2. Structure of ruthenium trisbipyridine $Ru(bpy)_3^{2+}$.

Upon excitation of $Ru(bpy)_3^{2+}$, an electron can be transferred from a metal orbital to a ligand orbital or from a ligand orbital to a metal orbital, resulting in transitions reflecting a metal-to-ligand charge transfer (MLCT) or a ligand-to-metal charge transfer (LMCT), respectively. The broad peak at 454 nm in the absorption spectrum of $Ru(bpy)_3^{2+}$ shown in

Figure 1.3 corresponds to an MLCT transition it is somewhat sensitive to solvent.[19,23] This solvent sensitivity has been suggested to result from the instantaneous response of the solvent to the formation of the dipolar excited state $[Ru(III)(bpy)_2(bpy^-)]^{2+}$ ion after a charge has been transferred from the metal to the ligand, as shown in Equation 1.1.[24]

$$[Ru^{II}(bpy)_3]^{2+} \xrightarrow{h\nu} [Ru^{III}(bpy)_2(bpy^-)]^{2+} \qquad 1.1$$

Excitation of $Ru(bpy)_3^{2+}$ at any wavelength of the absorption spectrum gives an emission peak around 610 nm.[24] A phenanthroline derivative of $Ru(bpy)_3^{2+}$, ruthenium (II) bisbipyridine-5-aminophenanthroline chloride ($RuNH_2$), will be used in this project.

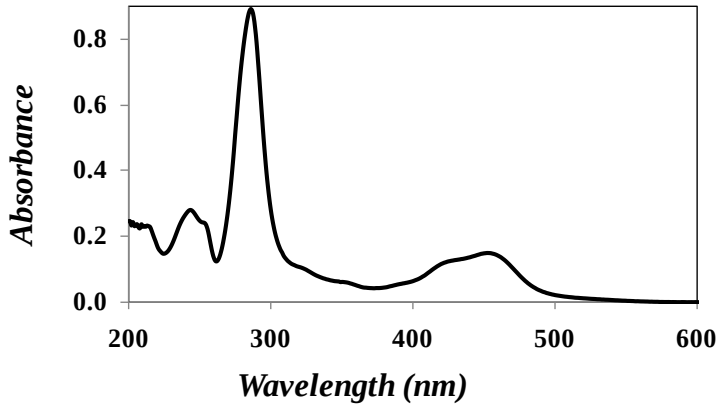

Figure 1.3. Absorption spectrum of $Ru(bpy)_3^{2+}$ $2Cl^-$ in a 0.1 M Na_2CO_3 solution (pH 9.6).

1.5. The Quencher: 1-Fluoro -2,4-Dinitrobenzene

1-Fluoro-2,4-dinitrobenzene (FDNB), also known as Sanger's reagent, is commonly used for polypeptide sequencing. Sanger first used it in 1945 to identify and determine the free amine end of insulin. By using FDNB and other techniques, he

successfully managed to sequence insulin and concluded that insulin is made up of two open peptide chains.[25] Sanger won the Nobel Prize for his work on protein structure determination in 1958. Since then, FDNB has been extensively used for studying proteins and polypeptides. FDNB reacts with the amine of amino acids to produce dinitrophenyl-amino acids. These DNP-amino acids are moderately stable under acid hydrolysis conditions that break peptide bonds. In the Sanger procedure, FDNB is used to form dinitrophenyl derivatives for end group determination of proteins, and to derivatize primary amines.[26] Although FDNB is not highly water-soluble, with a water-solubility of 8.6 mM at 15 °C,[27] this is still a lot better than that of 0.7 μM for pyrene at room temperature (23 °C).[28] FDNB's partial water-solubility, commercial availability, and ease of covalent attachment to an amine made it a suitable choice for this project. The structure of FDNB is shown in Figure 1.4.

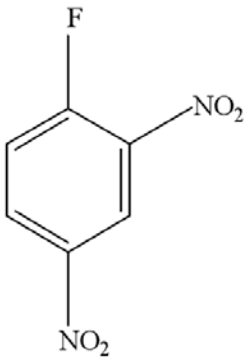

Figure 1.4. Structure of 1-fluoro-2,4-dinitrobenzene (FDNB).

1.6. The Polymer: Poly(*L*-lysine)

The water-soluble polymer used in this project was poly(*L*-lysine) (PLL) whose structure is shown in Figure 1.5. The amine side group of PLL can be used for covalent

attachment of the luminophore and quencher. Furthermore, PLL can adopt different conformations such as a random coil, α-helix, and β-sheet depending on the solution temperature and pH.[29]

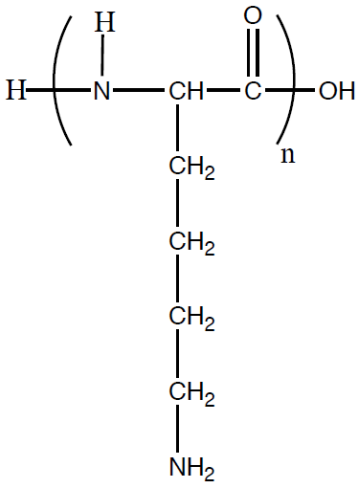

Figure 1.5. Structure of poly (*L*-lysine) (PLL).

In acidic aqueous solution, PLL is a polycation with a side chain containing a positively charged ammonium group. PLL is synthesized by a condensation reaction of the corresponding carboxy anhydride with the formation of peptide bonds between monomers. These bonds have a planar geometry that restricts the internal rotations of the PLL chain. The constraints induced by these peptide bonds and repulsion between the positive charges of the ammonium groups of the side chains lead PLL to adopt an open random-coil conformation at room temperature and acidic-to-neutral pH.[29] By increasing the pH of the solution, positively charged ammonium groups turn into neutral amines and PLL adopts an α-helical conformation,[30] which is stabilized by the formation of hydrogen bonds between every four lysine monomers constituting a helical turn. An increase in temperature causes an increase in the hydrophobicity of the side chains, leading PLL to adopt a β-sheet

conformation.[31] Since the formation of different secondary structures is expected to affect the LRPCD of a polypeptide, it would be thus interesting to study how LRPCD of PLL are affected by pH. Furthermore, the results obtained from PLL can be applied to more complex proteins, which can also adopt an α-helical conformation.

To understand how the conformation of PLL affects its LRPCD described by fluorescence measurements, the conformation of PLL needs to be characterized by a technique that yields structural information such as circular dichroism (CD). CD is widely used to investigate the secondary structure of proteins and polypeptides and monitor their change of conformation. CD measures the difference between the amount of right− and left−circulary polarized light being absorbed by a substance, and its expression is shown in Equation 1.2. CD spectra are typically reported in terms of the molar ellipiticity ([θ], in units of degrees.cm^2.dmol^{-1}) whose expression is shown in Equation 1.3.

$$CD = \theta_{obs} = \Delta A = A_L - A_R \qquad 1.2$$

$$[\theta] = \frac{(100 \times \theta_{obs})}{d \times m} \qquad 1.3$$

In Equation 1.3, *d* represents the path length of the cell and *m* is the molar concentration of the solution. The CD signal in the far-UV spectral region (190 to 250 nm) observed for a polypeptide solution can be analyzed to determine the amount and type of different secondary structures found in proteins such as α-helices, β-sheets, or random coils (Figure 1.6).

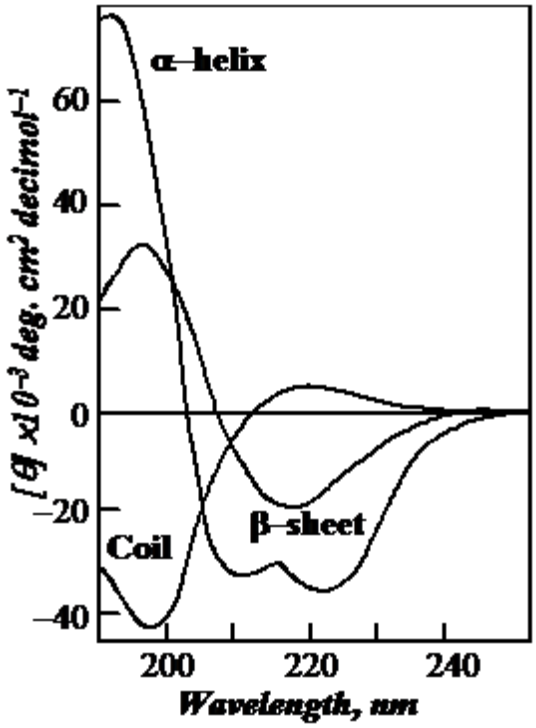

Figure 1.6. CD spectra of PLL under different conditions; α-helix in basic solution, β-sheet in neutral solution, and random coil in acidic solution and high temperature.[32]

Since the secondary structure of polypeptides is affected by solution conditions, e.g. temperature or pH, circular dichroism can be used to probe transitions in secondary structure. For instance, it is well-known that the CD spectrum of a random coil has a positive band around 220 nm and a negative band at 195 nm. The CD spectrum of a β-sheet has a negative and a positive band at 218 and 196 nm, respectively. The CD spectrum of an α-helix has a positive band at 192 and two negative bands at 209 and 222 nm. These spectral features can be used to assign the secondary structure of PLL. The CD spectra of PLL before and after attachment with the luminophore and quencher can also be compared to investigate how these labels affect the secondary structure of PLL.

1.7. Objective of the project

The objective of this project was to study the LRPCD of PLL randomly labeled with RuNCS and FDNB in aqueous solution as a function of solution pH. LRPCD were characterized by using time-resolved fluorescence and the FBM analysis and comparing the results obtained by fluorescence with the conformation of PLL characterized by CD. Furthermore, molecular mechanics optimizations with the Hyperchem modeling software (Hypercube, Inc) were carried out to ensure that the conclusions obtained experimentally by fluorescence and CD on the structure and internal dynamics of PLL were sound from a geometrical point of view.

2. Experimental

2.1. Materials

Unless otherwise stated, all chemicals were purchased from Sigma-Aldrich and were used without further purification. 5-Amino-1,10-phenanthroline was purchased from Polysciences, Inc. (Warrington, PA). Distilled in glass *N*,*N*-dimethylformamide (DMF) was obtained from Caledon (Georgetown, ON). Reagent grade ethanol and dialysis membrane (molecular weight cut-off = 2500 Daltons) were purchased from Fisher Scientific (Nepean, ON). Dialysis was performed using doubly distilled water (distilled from Millipore Milli-RO 10 Plus and Milli-Q UF Plus (Bedford, MA)).

2.2. Instrumentation

Steady-State Fluorescence Spectroscopy: Steady-state fluorescence spectra were acquired on a Photon Technology International fluorometer using the right angle geometry. Emission spectra were obtained by exciting the sample at 454 nm in 0.1 M aqueous sodium chloride solution. The solution absorption was set to equal ~ 0.2 at 454 nm, representing a concentration of ruthenium complex equal to or smaller than 20 μM, depending on whether quencher is present in the solution.

Time-Resolved Fluorescence Spectroscopy: The time-resolved fluorescence decays were obtained using the Time-Correlated Single Photon Counting (TCSPC) technique on an IBH time-resolved fluorometer. The fluorescence decays were acquired with the right angle geometry using a 460 nm nanoLED from HJY as the excitation source. The excitation and emission wavelengths were set to 454 and 610 nm, respectively. Possible stray light

scattered by the solution was eliminated by using a 550 nm cut-off filter. The slit-widths were set to 32 nm for both the excitation and emission. All decays were acquired with 20,000 counts at the maximum over 1,000 channels. A Ludox solution (colloidal silica suspension in water) was used to acquire the instrument response function.

Ultraviolet Absorption Measurements: Absorption spectra were obtained with a Cary 100 UV-Vis spectrophotomer. To ensure that the spectrophotometer was used within its linear response range, only absorption readings between 0.1 and 1.8 were considered.

Circular Dichroism: CD spectra were acquired on a J-715 CD spectropolarimeter (Jasco) at 25 °C with a 0.1 and 0.01 cm path length cell, a 100 nm/min scan rate, and a 2 nm bandwidth. The spectra were averaged over 10 scans from 190 to 250 nm. UV-Vis spectra were obtained before acquiring the CD spectra and the solution absorption was set to equal ~1.0 at 190 nm.

Nuclear Magnetic Resonance Spectroscopy (NMR): All NMR spectra were obtained on a Bruker Avance 300 MHz instrument. The spectrometer was equipped with either a Broadband Observed (bbo) 5 mm probe or a Quadruple Nucleus Probe (qnp) 5 mm probe. The samples were not spun during spectrum acquisition.

Mass Spectrometry: Positive ion nanoelectrospray (ESI) experiments were carried out on a Waters/Micromass QTOF Ultima Global mass spectrometer equipped with an electrospray ionizer and a quadrupole time-of-flight (QTOF) detector. Samples were infused at a rate of 2 μL/min in a 1:1 acetonitrile:water mixture. Typical operating conditions consisted of a source temperature of 80 °C, a capillary voltage of 3.5 kV, and a cone voltage of 60-160 V.

2.3. Synthetic procedures

2.3.1. Synthesis of the water-soluble dye Bis-(2,2-bipyridine)-ruthenium(II)-5-amino-1,10-phenanthroline hexafluorophosphate ($RuNH_2$)

$RuNH_2$ was synthesized by the coupling reaction of 5-amino-1,10-phenanthroline and *cis*-bis(bipyridyl) ruthenium (II) dichloride ($Ru(bpy)_2Cl_2$) by following the procedure of Ellis et al.[34,35] This reaction is shown in Scheme 2.1.

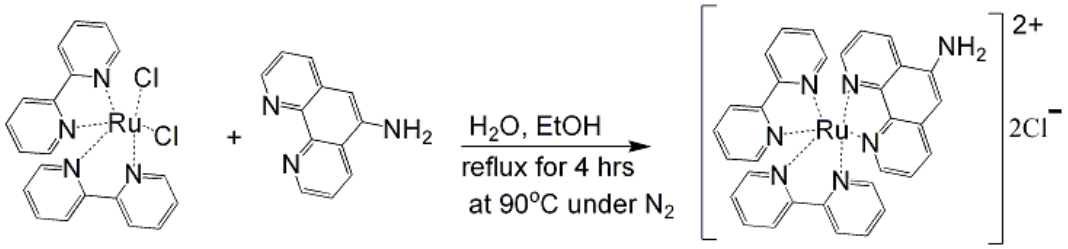

Scheme 2.1. Synthesis of $RuNH_2$

$Ru(bpy)_2Cl_2$ (0.060 mmol, 29 mg) was dissolved in 5 mL of milli-Q water at 60 °C and 5-amino-1,10-phenanthroline (0.071 mmol, 14 mg) was dissolved in 10 mL of ethanol at 40 °C. The two solutions were combined in a round bottom flask and degassed under N_2 at room temperature for half an hour and then refluxed at ~ 12 °C for four hours under N_2. Upon completion, ethanol was removed by rotary evaporation. Ammonium hexafluorophosphate (0.294 mmol, 48 mg) was added to the aqueous solution to replace the chloride ion and the solution was put in an ice bath for half an hour. The precipitate was then filtered and washed twice with 0.5 of mL Milli-Q water. It was dried in a vacuum oven at 100 °C for three hours and redissolved in a minimal amount of acetone to purify the product by passing through a neutral alumina column (1.5 cm diameter and 7 cm

height). A mixture of 1:2 toluene/acetonitrile was used as an eluent to retrieve the product from the column. The composition and the concentration of the collected fractions were determined by acquiring UV-vis absorption spectra for comparison to the starting materials, namely $Ru(bpy)_2Cl_2$ in Figure 2.1A and 5-amino-1,1-phenanthroline in Figure 2.1B, and that of the desired product, $RuNH_2$ in Figure 2.1C. The fractions having the desired absorption spectrum (Figure 2.1C) were concentrated by rotary evaporation and dried in a vacuum oven overnight. Recrystallization was performed as the final purification step by dissolving the product in a minimal amount of acetone and pouring it into cold ether with stirring. The product, $RuNH_2$ was finally dried in a vacuum oven overnight and a final yield of 87% was obtained.

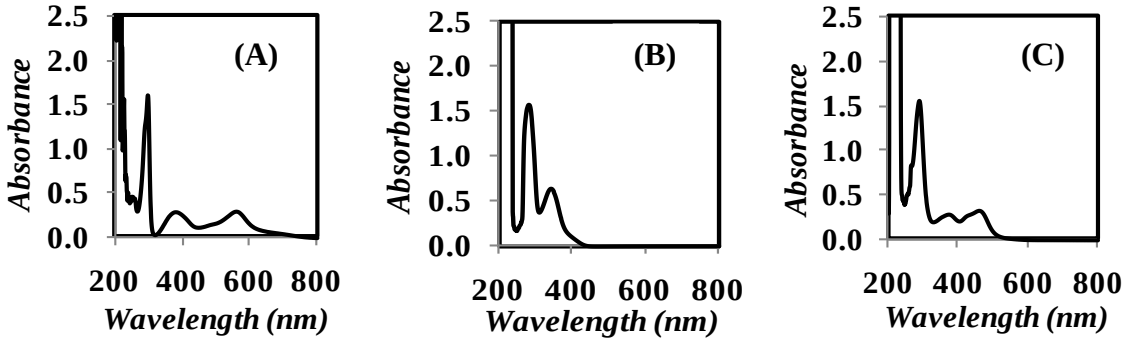

Figure 2.1. Absorption spectra for (A) $Ru(bpy)_2Cl_2$, (B) 5-amino-1,10-phenanthroline, and (C) $RuNH_2$ in DMF.

The ^1H NMR (Figure A.1) and mass (Figure A.2) spectra of $RuNH_2$ were obtained. The NMR spectrum shows the peaks corresponding to the aromatic protons of bipyridine and phenanthroline between 7.0 and 8.7 ppm. The amine protons of amino phenanthroline appear at 5.5 ppm.

^{1}H NMR (300 MHz, CD_3CN): δ = 8.60-7.15 (m, 23H, aromatic), 5.55 (s, 2H, NH_2)

The mass spectrum in Figure A.2 shows a large peak at 304.5 m/z which corresponds to $RuNH_2$ without any PF_6^- counter ions. The relatively smaller peak around 754 m/z is for $RuNH_2$ with one PF_6^- counter ion. Both of these peaks agree well with the expected m/z values of $RuNH_2$ without any PF_6^- counter ions (304.5 m/z) and with one PF_6^- counter ion (754 m/z).

Bis-(2,2-bipyridine)-ruthenium(II)-5-isothiocyanato-1,10-phenanthroline chloride (RuNCS)

Since the amine substituent on the phenanthroline ring cannot be directly attached to poly(*L*-lysine) (PLL), it was converted into an isothiocyanate using thiophosgene. The procedure used by Ryan et al.[34,35] and depicted in Scheme 2.1 was closely followed for this modification.

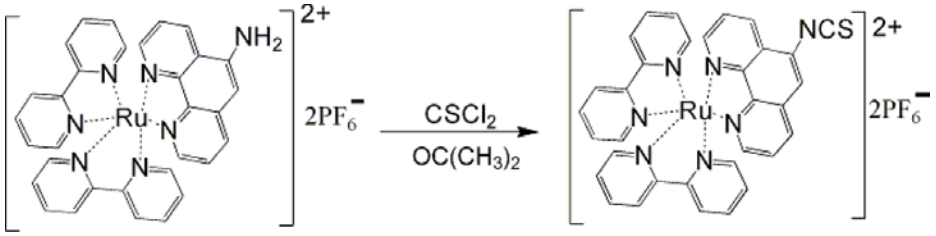

Scheme 2.1. Synthesis of RuNCS.

$RuNH_2$ (0.3 mmol, 227 mg) was dissolved in a minimal amount of freshly distilled acetone and added to a flame dried round bottom flask. After degassing the solution for half an hour under a gentle flow of dry N_2, 92 μL of thiophosgene in 5 mL of acetone was added dropwise over half an hour while the round bottom flask was cooled in an ice-water

bath. The solution was stirred at room temperature for 24 hours in the dark under a gentle flow of N_2. The acetone was then removed by rotary evaporation and the product was dried in a vacuum oven for three hours. In order to solubilize the product in aqueous solution, the counter ion hexafluorophosphate was replaced with a chloride ion by adding ~7 mL of Milli-Q water and ~ 500 mg Amberlite IRA 400 (Cl) ion exchange resin to the product and letting the mixture stir for two hours. The solution was filtered to remove the resin, which was washed three times with 0.5 mL of Milli-Q water. The filtrate was concentrated by rotary evaporation and dried in a vacuum oven at 65 °C for three hours. A final yield of 80% was achieved. The ^{1}H NMR (Figure A.3) and mass (Figure A.4) spectra were obtained. The ^{1}H NMR spectrum shows no amine peak around 5.5 ppm as was previously observed for $RuNH_2$ (Figure A.1). This observation implies that $RuNH_2$ has been successfully converted to RuNCS. The mass spectrum shows a large peak at 325.5 m/z which corresponds to RuNCS without any PF_6^- counter ions. The smaller peak around 796.0 m/z corresponds to RuNCS with one PF_6^- counter ion. Both of these peaks agree well with the expected m/z values of RuNCS without any PF_6^- counter ions (325.5 m/z) and with one PF_6^- counter ion (796.0 m/z).

^{1}H NMR (300 MHz, CD_3CN): δ = 8.75-7.25 (m, 23H, aromatic)

2.3.2. PLL Labeling

PLL (M_n = 15000-3000) was labeled with RuNCS and dinitrobenzene by using the procedure described by Ryan et al.[35] The structure of the labeled PLL is shown in Figure 2.2. In this scheme *m* and *k* are the mole fractions of the chromophore and quencher,

respectively, while *n* is the mole fraction of unlabeled lysine monomer. Mole fractions of 0.02, 0.01-0.10 and 0.88-0.97 were targeted for *m*, *k*, and *n*, respectively.

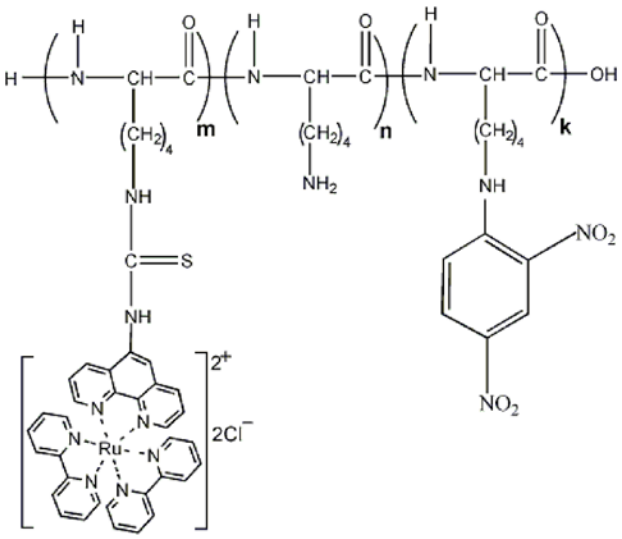

Figure 2.2. Structure of PLL randomly labeled with the chromophore and quencher.

Labeling of PLL with RuNCS

The procedure of Ryan et al.[35] was used to label PLL with RuNCS and is shown in Scheme 2.2. First, PLL HCl (0.15 mmol, 25 mg) was dissolved in 2 mL of 0.1 M Na_2CO_3 solution (pH 9.6). RuNCS (0.075 mmol, 47 mg) was then dissolved in 3 mL of a 4:1 mixture of DMF and a 0.1 M Na_2CO_3 solution, which was added dropwise to the PLL solution. The conjugation reaction proceeded overnight at 4 °C in the dark, yielding the ruthenium labeled PLL (Ru-PLL). Dialysis (6-7 hours per run) against milli-Q water was performed repeatedly (usually 3 times) until no free lumniophore could be detected by UV-Vis absorption. The product was lyophilized with a freeze drier and the Ru content of this sample was characterized by UV-Vis absorption and found to yield an *m* and *n* values equal to 0.018 and 0.982, respectively.

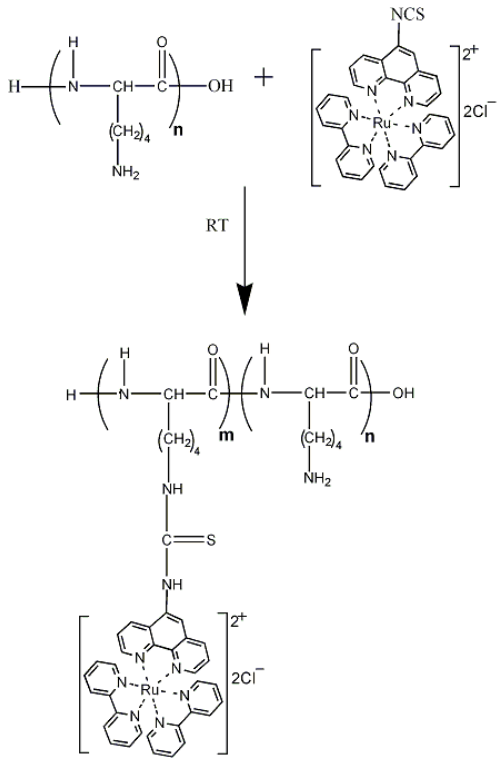

Scheme 2.2. Labeling of PLL with RuNCS to yield Ru-PLL.

Labeling of Ru-PLL with FDNB

Ru-PLL was then labeled with 1-fluoro-2,4-dinitrobenzene (FDNB)[36] according to Scheme 2.3. Ru-PLL (30 mg) was dissolved in 0.6 mL of milli-Q water, to which 0.4 mL of ethanol and 0.04 mL of triethylamine were added. Finally, 10 μL of FDNB in 0.8 mL of ethanol was added with swirling. The reaction mixture was covered in aluminum foil and kept in the dark at room temperature for 48 hours. The product was dialyzed several times against a 1:2 milli-Q water:ethanol mixture to remove unbound FDNB. Then water and ethanol were removed using a rotary evaporator. The product was dissolved in water to be

lyophilized with a freeze drier to yield PLL randomly labeled with the ruthenium complex and dinitrobenzene (Ru-PLL-Q).

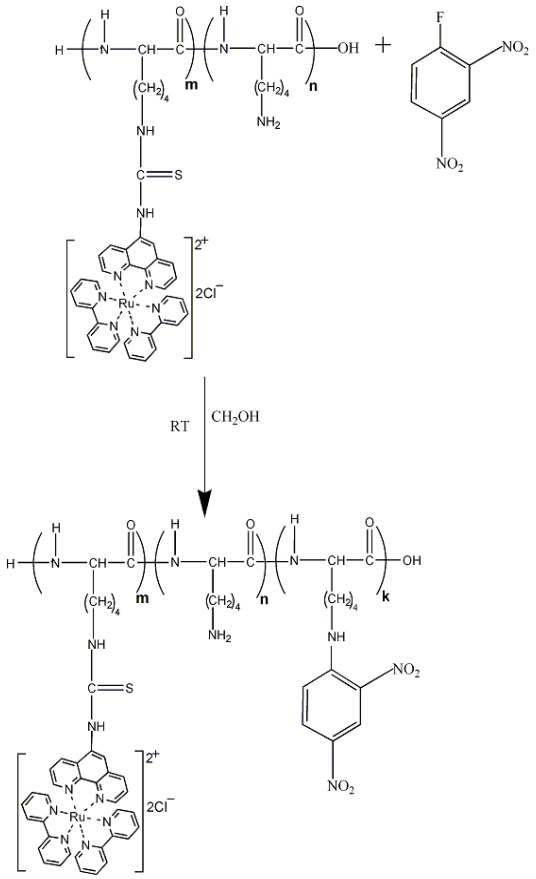

Scheme 2.3. Labeling of Ru-PLL with FDNB to yield Ru-PLL-Q.

The composition of Ru-PLL-Q was determined by UV-Vis absorption according to a procedure which is described in Section 4. In the case of this specific synthesis, *m*, *n*, and *k* were found to equal 0.02, 0.95, and 0.03 respectively.

2.3.3. Ru and Dinitrobenzene Content Determination

Ru Content Determination

After the Ru-PLL synthesis was completed, the luminophore content, λ_{Ru}, expressed in mol.g^{-1}, was obtained by comparing the absorption of a solution of Ru-PLL with the molar absorption coefficient of $RuNH_2$. The concentration of the Ru complex attached to the polypeptide was determined by dissolving a known mass of Ru-PLL (m) in a known volume of solvent (V) and acquiring the absorption spectrum of the solution. The Beer-Lambert law whose expression is shown in Equation 2.1 was then applied at 454 nm to determine the luminophore concentration in the solution.

$$Abs = \varepsilon[Ru]L \qquad 2.1$$

In Equation 2.1, L is the cell path length of the detection beam equal to 1 cm. The molar absorption coefficient, ε, of $RuNH_2$ at 454 nm has been reported to equal 13,800 M^{-1}.cm^{-1} in a 0.1 M Na_2CO_3 solution at pH 9.6.[35] Equation 2.2 is then used to determine the luminophore content λ_{Ru} of the labeled polypeptide expressed in moles of luminophore per gram of polypeptide.

$$\lambda_{Ru} = \frac{[Ru]}{m/V} \qquad 2.2$$

The mole fraction (x_{Ru}) of the luminophore-labeled PLL monomer is calculated by using Equation 2.3,

$$x_{Ru} = \frac{\lambda_{Ru} M}{1 - \lambda_{Ru}(M_{Ru} - M)} \qquad 2.3$$

where M and M_{Ru} represent the molar masses of the PLL structural units that are not labeled (146 g/mol) and labeled with luminophore (868 g/mol), respectively.

Ru and Dinitrobenzene Content Determination

The determinination of the Ru content, λ_{Ru}, and DNB content, λ_Q, for a Ru-PLL-Q sample was complicated by the fact that both Ru-PLL and Q-PLL absorb in the same region of the UV-Vis spectrum, as shown in Figure 2.3.

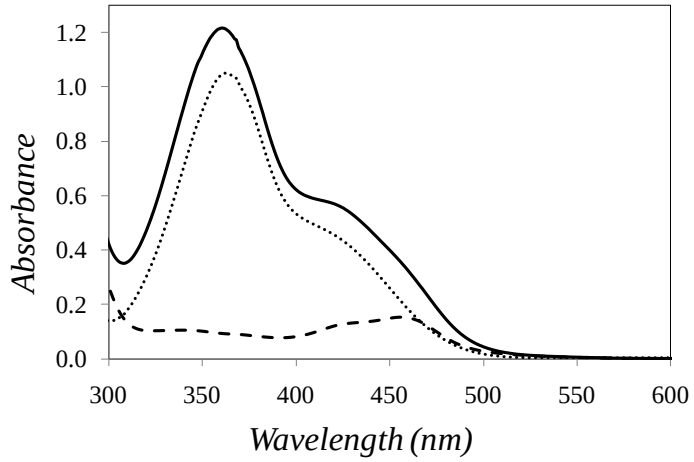

Figure 2.3. Absorption spectrum of Ru-PLL-Q (——) which was decomposed into Ru-PLL (------) and Q-PLL (·····) by optimization.

λ_{Ru} and λ_Q were obtained by comparing the absorption of a solution of Ru-PLL-Q with the molar absorption coefficients of $RuNH_2$ and *N*-(2,4-dinitrophenyl)-*L*-lysine

hydrochloride which was used as a model compound for PLL-Q. The concentration of the luminophore and quencher attached to the polypeptide was determined by dissolving a known amount of labeled polymer (*m*) in a known volume of solvent (*V*) and acquiring the absorption spectrum of the solution. The Beer-Lambert law, whose expression (assuming a path length *L* equal to 1 cm) is shown in Equation 2.4 at a given wavelength λ_i, was then applied over a range of wavelength (400 - 500 nm) to determine the luminophore and quencher concentration of the Ru-PLL-Q solution.

$$Abs(\lambda_i) = \varepsilon_{Ru}(\lambda_i)[Ru] + \varepsilon_Q(\lambda_i)[Q] \qquad 2.4$$

In Equation 2.4, the absorbance, Abs(λ_i), molar absorption coefficients for Ru, $\varepsilon_{Ru}(\lambda_i)$, and FDNB, $\varepsilon_Q(\lambda_i)$, are known but the concentrations [Ru] and [Q] are unknown. To determine the concentrations [Ru] and [Q] that would best represent the function Abs(λ_i) in Equation 2.4, the merit function S given in Equation 2.5 was minimized.

$$S = \sum_{i=1}^{N} \{Abs(\lambda_i) - \varepsilon_{Ru}(\lambda_i)[Ru] - \varepsilon_Q(\lambda_i)[Q]\}^2 \qquad 2.5$$

Minimization of S with respect to [Ru] and [Q] yielded Equations 2.6 and 2.7 which were set to equal zero.

$$\frac{\partial S}{\partial [Ru]} = 0 = 2\sum_{i=1}^{N} \{Abs(\lambda_i) - \varepsilon_{Ru}(\lambda_i)[Ru] - \varepsilon_Q(\lambda_i)[Q]\}\varepsilon_{Ru}(\lambda_i) \qquad 2.6$$

$$\frac{\partial S}{\partial [Q]} = 0 = 2\sum_{i=1}^{N} \{Abs(\lambda_i) - \varepsilon_{Ru}(\lambda_i)[Ru] - \varepsilon_Q(\lambda_i)[Q]\}\varepsilon_Q(\lambda_i) \qquad 2.7$$

Equations 2.6 and 2.7 can be rearranged into Equations 2.8 and 2.9, which constitute a set of two equations with two unknowns, namely [Ru] and [Q].

$$\sum \varepsilon_{Ru}(\lambda_i)\varepsilon_Q(\lambda_i)[Ru] + \sum \varepsilon_Q{}^2(\lambda_i)[Q] = \sum Abs(\lambda_i)\varepsilon_Q(\lambda_i) \qquad 2.8$$

$$\sum \varepsilon_{Ru}{}^2(\lambda_i)[Ru] + \sum \varepsilon_Q(\lambda_i)\varepsilon_{Ru}(\lambda_i)[Q] = \sum Abs(\lambda_i)\varepsilon_{Ru}(\lambda_i) \qquad 2.9$$

The quantities A_{11}, A_{12}, A_{22}, B_1, and B_2 are introduced in Equations 2.10-2.14 to provide a more concise form of the solution set ([Ru], [Q]) that solves the set of Equations 2.8 and 2.9.

$$\sum \varepsilon_{Ru}{}^2(\lambda_i) = A_{11} \qquad 2.10$$

$$\sum \varepsilon_Q(\lambda_i)\varepsilon_{Ru}(\lambda_i) = A_{12} \qquad 2.11$$

$$\sum Abs(\lambda_i)\varepsilon_{Ru}(\lambda_i) = B_1 \qquad 2.12$$

$$\sum \varepsilon_Q{}^2(\lambda_i) = A_{22} \qquad 2.13$$

$$\sum Abs(\lambda_i)\varepsilon_Q(\lambda_i) = B_2 \qquad 2.14$$

The expressions of [Ru] and [Q] are given in Equations 2.15 and 2.16.

$$[Ru] = \frac{B_1A_{22} - B_2A_{12}}{A_{11}A_{22} - A_{12}{}^2} \qquad 2.15$$

$$[Q] = \frac{B_1A_{12} - B_2A_{11}}{A_{11}A_{22} - A_{12}{}^2} \qquad 2.16$$

The concentrations [Ru] and [Q] can then be used to determine λ_{Ru} and λ_Q for the Ru-PLL-Q solution containing a mass (m) of labeled polymer in a volume (V) of milli-Q water. The expressions of λ_{Ru} and λ_Q are given in Equations 2.17 and 2.18, respectively. The molar fractions of lysine labeled with Ru (x_{Ru}) and Q (x_Q) can then be determined by, respectively, Equations 2.19 and 2.20 where M and M_{Ru} have already been defined and M_Q equals the molar mass of a DNB-labeled lysine (313 g.mol^{-1}).

$$\lambda_{Ru} = \frac{x_{Ru}}{M_Q x_Q + M_{Ru} x_{Ru} + (1 - x_Q - x_{Ru})M} \qquad 2.17$$

$$\lambda_Q = \frac{x_Q}{M_Q x_Q + M_{Ru} x_{Ru} + (1 - x_Q - x_{Ru})M} \qquad 2.18$$

$$x_{Ru} = \frac{\lambda_{Ru} M}{1 - \lambda_Q (M_Q - M) - \lambda_{Ru} (M_{Ru} - M)} \qquad 2.19$$

$$x_Q = \frac{\lambda_Q M}{1 - \lambda_Q (M_Q - M) - \lambda_{Ru} (M_{Ru} - M)} \qquad 2.20$$

The values of x_{Ru} and x_Q for different PLL samples labeled with Ru and Q (Ru-PLL-Q) are given in Table 2.1. Table 2.1 shows that λ_{Ru} does not change significantly from Ru-PLL to Ru-PLL-Q, which confirms that labeling Ru-PLL with DNB does not affect λ_{Ru} much.

Table 2.1. A) Luminophore content for different Ru-PLL samples, **B)** Luminophore and quencher for different Ru-PLL-Q samples.

2.1A

Sample	$x_{Ru\text{-}1}$ ×100	$\lambda_{Ru\text{-}1}$ µmol/g
$Ru_{0.6}$-PLL	0.6	36
$Ru_{2.5}$-PLL	2.5	125
$Ru_{1.5}$-PLL	1.5	85
$Ru_{0.9}$-PLL	0.9	58
$Ru_{2.0}$-PLL	2.0	107
$Ru_{1.2}$-PLL	1.2	86
$Ru_{1.0}$-PLL	1.0	53
$Ru_{1.6}$-PLL	1.6	82
$Ru_{2.6}$-PLL	2.6	135
$Ru_{2.2}$-PLL	2.2	112
$Ru_{2.1}$-PLL	2.1	97

2.1B

Sample	$x_{Ru\text{-}2}$ ×100	$\lambda_{Ru\text{-}2}$ µmol/g	x_{Q} ×100	λ_{Q} µmol/g
$Ru_{0.6}$-PLL-$Q_{2.7}$	0.4	30	2.7	178
$Ru_{2.5}$-PLL-$Q_{3.3}$	2.3	113	3.4	180
$Ru_{1.5}$-PLL-$Q_{3.4}$	1.2	71	3.4	181
$Ru_{0.9}$-PLL-$Q_{4.9}$	0.7	47	4.9	315
$Ru_{2.0}$-PLL-$Q_{5.3}$	2.0	100	5.3	280
$Ru_{1.2}$-PLL-$Q_{5.9}$	1.2	74	5.9	376
$Ru_{1.0}$-PLL-$Q_{7.1}$	0.8	41	7.1	369
$Ru_{1.6}$-PLL-$Q_{8.4}$	1.4	74	8.4	432
$Ru_{2.6}$-PLL-$Q_{11.0}$	2.5	127	10.9	557
$Ru_{2.2}$-PLL-$Q_{11.5}$	1.9	100	11.5	583
$Ru_{2.1}$-PLL-$Q_{12.1}$	2.1	105	12.1	612

2.4. Analysis

Analysis of the Fluorescence Decays

The fluorescence decays were first fitted with a sum of 2-3 exponentials given in Equation 2.21 after convolution with the instrument response function.[37]

$$i_{Ru}(t) = \sum_{i=1}^{n} a_i \exp(-t/\tau_i) \qquad 2.21$$

The fluorescence decays of the Ru-PLL-Q samples were also fitted according to the FBM using Equation 2.22 to yield the parameters A_2, A_3, A_4, and f_{diff}.

$$i_{Ru}(t) = f_{diff} \exp\{-(A_2)t - A_3[1-\exp(-A_4 t)]\}F_{Ru}(t) + (1-f_{diff})F_{Ru}(t) \qquad 2.22$$

$$A_2 = < n > \frac{k_{blob}k_e[blob]}{k_{blob}+k_e[blob]} \quad A_3 = < n > \frac{{k_{blob}}^2}{(k_{blob}+k_e[blob])^2} \quad A_4 = k_{blob}+k_e[blob] \qquad 2.23$$

F_{Ru}(t) in Equation 2.22 represents the natural decay of the Ru label when no quencher was attached to PLL. F_{Ru}(t) was either a bi- or a triexponential function whose decay times and pre-exponential factors were fixed when the fluorescence decays of Ru-PLL-Q were fitted with Equation 2.22. In practice, F_{Ru}(t) was taken to equal i_{Ru}(t) used to fit the fluorescence decay of the Ru-PLL sample from which a given Ru-PLL-Q sample was obtained. The parameters A_2, A_3, and A_4 in Equations 2.23 are functions of k_{blob}, the rate constant of encounter between a quencher and an excited ruthenium inside a blob, k_e, the rate constant for the exchange of quenchers between blobs, [*blob*], the concentration of blobs inside the

polymer coil, and <*n*>, the average number of quenchers per blob. The parameter f_{diff} represents the fraction of luminophores quenched by diffusive encounters with a quencher. The value of f_{diff} is used to determine N_{blob}, the number of monomer units per blob by using Equation 2.24.

$$N_{blob} = \frac{< n >}{(\lambda_Q / f_{diff})[M_Q x_Q + M_{Ru} x_{Ru} + M(1 - x_Q - x_{Ru})} \qquad 2.24$$

In Equation 2.24, λ_{Q} is the quencher content of the polypeptide, while M_Q, M_{Ru}, and M are the molar masses of a lysine bearing a quencher (313 g/mol), bearing a luminophore (868 g/mol), or nothing (146 g/mol), respectively. The fractions x_Q and x_{Ru} are the molar fractions of the lysines bearing a quencher and a luminophore, respectively. λ_{Ru}, λ_{Q}, x_{Ru}, and x_Q are given in Tables 2.1A and 2.1B.

3. Results and Discussion

3.1. Characterization of the products

After the water-soluble luminophore $RuNH_2$ was synthesized, its photophysical properties were characterized by UV-Vis absorption and steady-state and time-resolved fluorescence and compared to the results obtained in earlier studies.[35] Figure 3.1 shows the UV-Vis absorption and emission spectra of $RuNH_2$ in 0.1 M Na_2CO_3 aqueous solution at pH 9.6. The absorption and emission bands at, respectively, 454 and 610 nm, match well with reported values.[35]

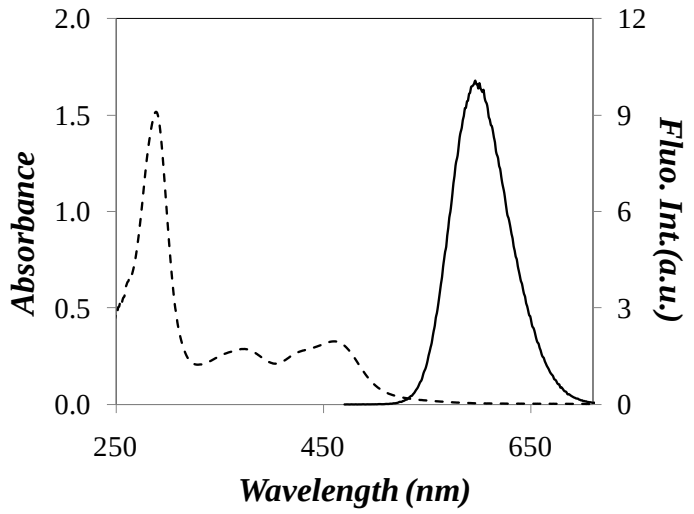

Figure 3.1. Absorption (·····) and emission (——, λ_{ex}= 454 nm) spectra of 20 μM $RuNH_2$ in a 0.1 M Na_2CO_3 aqueous solution at pH 9.6. The solution was degassed to acquire the emission spectrum.

The molar absorption coefficient of $RuNH_2$ in a 0.1 M Na_2CO_3 solution at pH 9.6 was found to equal 13,700 ± 100 $M^{-1}cm^{-1}$ at 454 nm, which agreed well with the reported value of 13,800 $M^{-1}cm^{-1}$.[35] The fluorescence decay of a degassed $RuNH_2$ aqueous solution

in 0.1 M Na_2CO_3 at pH 9.6 was obtained by time-resolved fluorescence using the single photon counting technique. The decay appeared monoexponential as shown in Figure 3.2 but needed to be fitted with a biexponential function yielding a χ^2 of 1.08. The decay times with their associated pre-exponential factors given in parenthesis were found to equal 713 ns (0.87) and 365 ns (0.13) yielding a number-average lifetime $<\tau>_N$ of 667 ns. The lifetime of $RuNH_2$ in a 0.1 M Na_2CO_3 aqueous solution at pH 9.6 has been reported to equal 639 ns for a monoexponential decay.[35] Thus the average lifetime obtained for the decay shown in Figure 3.2 compares well with the reported lifetime of $RuNH_2$. However, the origin of the biexponential decay of $RuNH_2$ has not been elucidated.

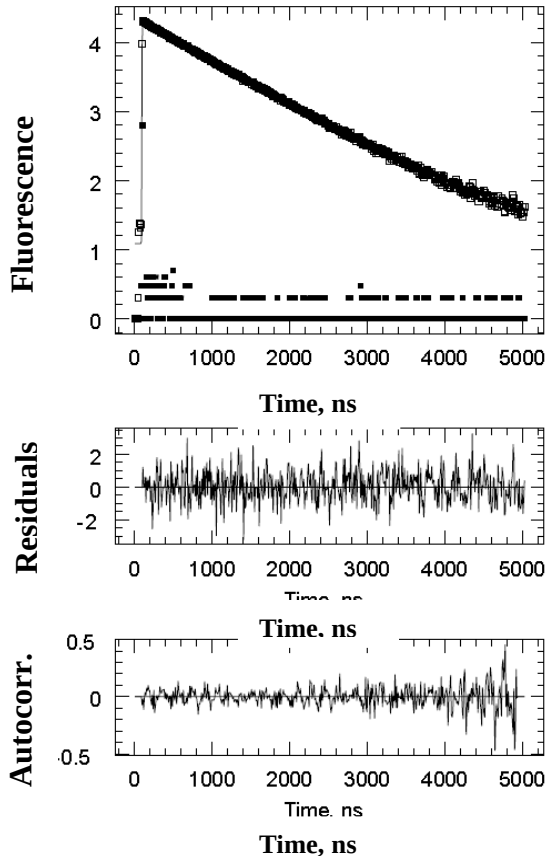

Figure 3.2. Fluorescence decay of a 20 μM $RuNH_2$ in a 0.1 M Na_2CO_3 aqueous solution at pH 9.6.; λ_{ex}= 454 nm and λ_{em}= 610 nm. The solution was degassed.

Next, $RuNH_2$ was converted to RuNCS and attached onto PLL. The photophysical properties of PLL labeled with RuNCS (Ru-PLL) were characterized. Figure 3.3 shows the UV-Vis absorption and emission spectra of the labeled PLL in a 0.1 M Na_2CO_3 aqueous solution at pH 9.6. Beside the weak absorption band at 360 nm in Figure 3.1, both absorption and emission spectra of the labeled PLL resemble closely those of $RuNH_2$ shown in Figure 3.1.

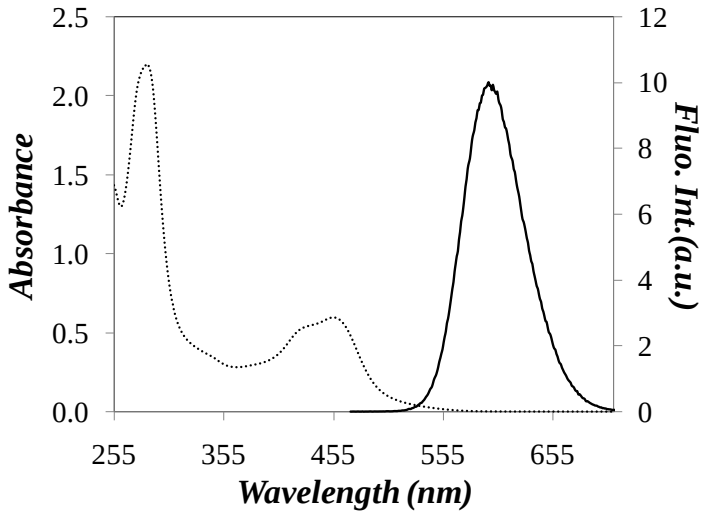

Figure 3.3. Absorption (·····) and emission (———; λ_{ex}= 454 nm) spectra of $Ru_{2.6}$-PLL in a 0.1 M Na_2CO_3 aqueous solution at pH 9.6 [$Ru_{2.6}$-PLL] = 20 μM. The solution was degassed to acquire the emission spectrum.

The fluorescence decay of a 20 μM Ru-PLL in a degassed aqueous solution was fitted with Equation 2.21 to get a triexponential decay as shown in Figure 3.4. The decay times with pre-exponential factors given in parenthesis were 163 ns (0.18), 434 ns (0.59), and 818 ns (0.23) yielding a $<\tau>$ value of 478 ns with a χ^2 of 1.03. It is not clear at this

point if this decrease in RuNCS lifetime is due to its attachment to PLL, resulting in its possible quenching by the primary amines of the side chain, or by a self-quenching mechanism with a neighboring RuNCS luminophore. The decay shown in Figure 3.4 was for the $Ru_{2.6}$-PLL sample in Table 2.1A where 2.6 represents the ruthenium content of the sample in mol%.

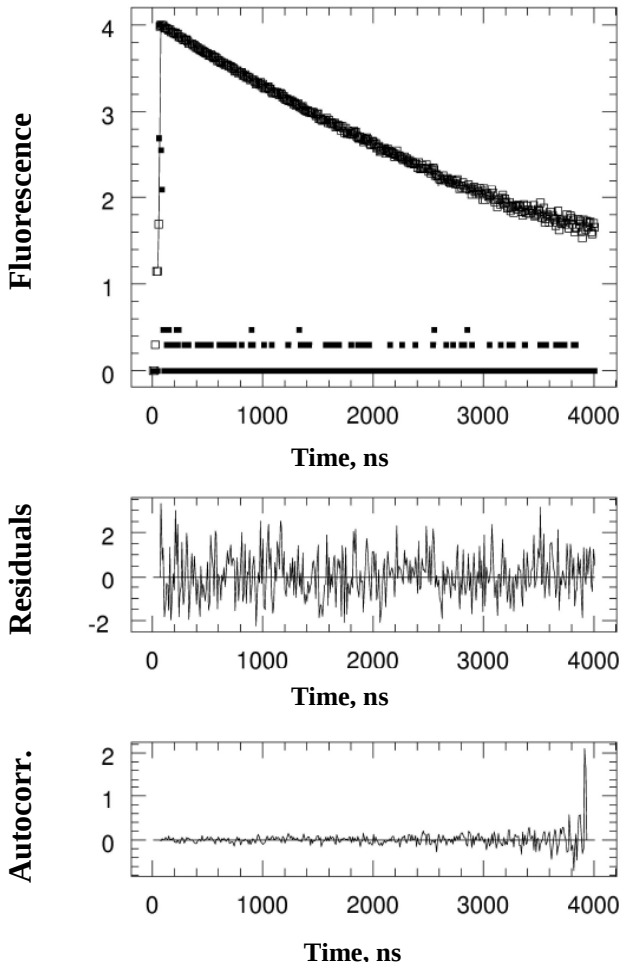

Figure 3.4. Fluorescence decay of 20 μM $Ru_{2.6}$-PLL in a degassed aqueous solution (λ_{ex}= 454 nm and λ_{em}= 610 nm).

Different Ru-PLL samples were synthesized and characterized. They were found to yield decays having different number-average lifetimes $<\tau>_N$ which might be due to differences in the batches of RuNCS used to label PLL, the Ru content of the Ru-PLL samples, the local environments provided by PLL to the Ru label, or a combination of all three possible effects. The number-average lifetimes determined for all Ru-PLL samples studied are listed with their PDI's in Table 3.1A. PDI is the polydispersity index of a fluorescence decay and it equals $<\tau>_W/<\tau>_N$, where $<\tau>_W$ is the weight-average lifetime. The expressions of PDI, $<\tau>_W$, and $<\tau>_N$ are shown in the Equations 3.1, 3.2, and 3.3, respectively.

$$PDI = \frac{<\tau>_W}{<\tau>_N} \qquad 3.1$$

$$<\tau>_W = \frac{\sum a_i \tau_i^{\,2}}{\sum a_i \tau_i} \qquad 3.2$$

$$<\tau>_N = \frac{\sum a_i \tau_i}{\sum a_i} \qquad 3.3$$

The decay times τ_i and pre-exponential factors a_i used in Equation 3.2 and 3.3 are retrieved from the multiexponential fits of the decays with Equation 2.21.

Table 3.1. Number-average lifetime and PDI for different A) Ru-PLL and B) Ru-PLL-Q samples.

3.1A

Sample	$\langle\tau\rangle_N$	PDI
$Ru_{0.6}$-PLL	767	1.07
$Ru_{2.5}$-PLL	1283	1.05
$Ru_{1.5}$-PLL	883	1.04
$Ru_{0.9}$-PLL	635	1.13
$Ru_{2.0}$-PLL	559	1.15
$Ru_{1.2}$-PLL	689	1.09
$Ru_{1.0}$-PLL	586	1.10
$Ru_{1.6}$-PLL	619	1.09
$Ru_{2.6}$-PLL	478	1.20
$Ru_{2.2}$-PLL	577	1.02
$Ru_{2.1}$-PLL	535	1.13

3.1B

Sample	$\langle\tau\rangle_N$	PDI
$Ru_{0.6}$-PLL-$Q_{2.7}$	583	1.41
$Ru_{2.5}$-PLL-$Q_{3.3}$	1075	1.18
$Ru_{1.5}$-PLL-$Q_{3.4}$	811	1.29
$Ru_{0.9}$-PLL-$Q_{4.9}$	410	1.40
$Ru_{2.0}$-PLL-$Q_{5.3}$	395	1.41
$Ru_{1.2}$-PLL-$Q_{5.9}$	379	1.49
$Ru_{1.0}$-PLL-$Q_{7.1}$	319	1.55
$Ru_{1.6}$-PLL-$Q_{8.4}$	284	1.50
$Ru_{2.6}$-PLL-$Q_{11.0}$	253	2.07
$Ru_{2.2}$-PLL-$Q_{11.5}$	406	1.38
$Ru_{2.1}$-PLL-$Q_{12.1}$	332	1.47

Although a sum of 2-3 exponentials was needed to fit the Ru-PLL fluorescence decays, all PDI's listed in Table 3.1A are smaller than 1.20, a number that remains close to unity indicating that the Ru-PLL decays are dominated by a single pathway. After the synthesis and characterization of the Ru-PLL samples, the Ru-PLL-Q samples were synthesized following the procedure outlined in Section 2.3 and their quencher and ruthenium content were determined. Hence the ruthenium content of each Ru-PLL-Q sample was determined twice, before and after the quencher attachment. Both of these ruthenium contents were found to be very close, as shown in Table 2.1A and 2.1B.

Figure 3.5 compares the UV-Vis absorption spectra of the Ru-PLL and Ru-PLL-Q samples before and after the quencher attachement to PLL, respectively. An additional peak is clearly observed around 362 nm in the Ru-PLL-Q absorption spectrum as compared to that of Ru-PLL. The peak at 362 nm results from the attachment of the DNB quencher to Ru-PLL. The peak for ruthenium still appears at 454 nm, which shows that the addition of quencher to Ru-PLL did not affect the absorbance of the ruthenium complex. Furthermore, the ruthenium contents found for Ru-PLL and Ru-PLL-Q were very close. The UV-Vis spectra shown in Figure 3.5 are for the samples $Ru_{2.6}$-PLL and $Ru_{2.5}$-PLL-Q_{11}, where 2.6 and 2.5 are the molar percentages of the ruthenium-labeled lysines before and after quencher attachment, respectively, and 11 is the molar percentage of quencher-labeled lysines.

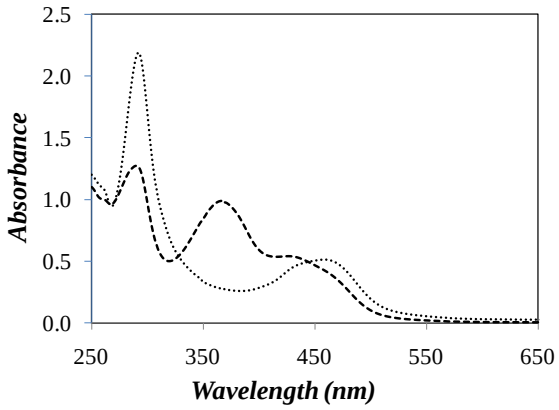

Figure 3.5. Absorption spectra of 4 μM $Ru_{2.6}$-PLL (.....) and 0.2 μM $Ru_{2.5}$-PLL-Q_{11} (- - - -) in milli-Q water. Concentrations are given with respect to the Ru-label.

A model compound, *N*-dinitrophenyl-*L*-(lysine) hydrochloride (DNPL) was used to determine the DNB content of the Ru-PLL-Q samples. The molar absorption coefficient of

DNPL in milli-Q water was found to equal 15,800 ± 100 $M^{-1}cm^{-1}$ at 362 nm, which agreed well with the reported value of 15,900 $M^{-1}cm^{-1}$.[38]

Next, the fluorescence decays of the Ru-PLL-Q samples were acquired in a degassed aqueous solution and compared to those of Ru-PLL, as was done in Figure 3.6 for $Ru_{2.6}$-PLL and $Ru_{2.5}$-PLL-Q_{11}. The fluorescence decay of $Ru_{2.6}$-PLL was the same as the one shown in Figure 3.4 with a $<\tau>_N$ value of 478 ns. The decay of $Ru_{2.5}$-PLL-Q_{11} exhibits a strong curvature as compared to that of $Ru_{2.6}$-PLL because of quenching by DNB. The triexponential analysis of the $Ru_{2.5}$-PLL-Q_{11} decay yielded a good fit with a χ^2 of 1.14. The decay times of 48, 243, and 693 ns with associated pre-exponential factors of, respectively, 0.48, 0.30, and 0.22 were retrieved resulting in a $<\tau>_N$ value of 253 ns.

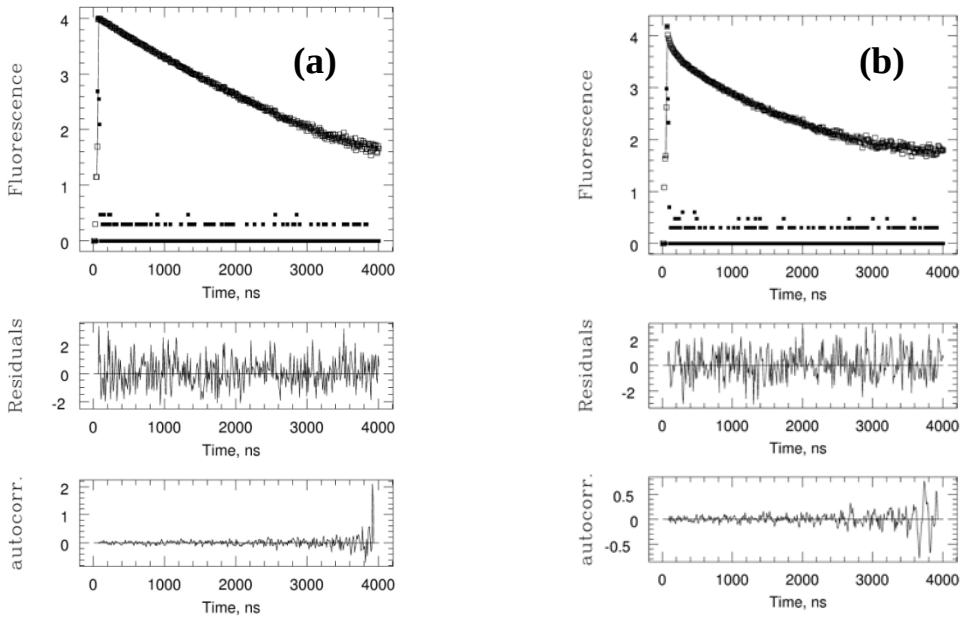

Figure 3.6. Fluorescence decays of a) $Ru_{2.6}$-PLL and b) $Ru_{2.5}$-PLL-Q_{11} in a degassed aqueous solution (λ_{ex}= 454 nm and λ_{em}= 610 nm).

The decrease in $<\tau>_N$ for $Ru_{2.6}$-PLL from 478 ns to 253 ns after quencher attachment demonstrates that quenching is taking place. The $<\tau>_N$ values and PDI's for the Ru-PLL-Q samples are given in Table 3.1B. The decay times for Ru-PLL and Ru-PLL-Q samples with their associated pre-exponential factors and χ^2 are given in Tables A.1 and A.2 in the Appendix, respectively. Whereas all PDI's obtained for the Ru-PLL samples were smaller than 1.20, the PDI's in Table 3.1B for the Ru-PLL-Q samples having a quencher content greater than 4 mol% were all larger than 1.30. These larger PDI's indicate that the decays adopt a more strongly multiexponential character reflecting quenching by the DNB species randomly distributed along the PLL backbone.

In order to describe the extent of quenching more quantatively, the ratio *Q* was introduced. *Q* is the ratio of $<\tau>_N$ of Ru-PLL over $<\tau>_N$ of Ru-PLL-Q. It is plotted against the quencher content in Figure 3.7 and it is expected to increase with the increasing quencher content.

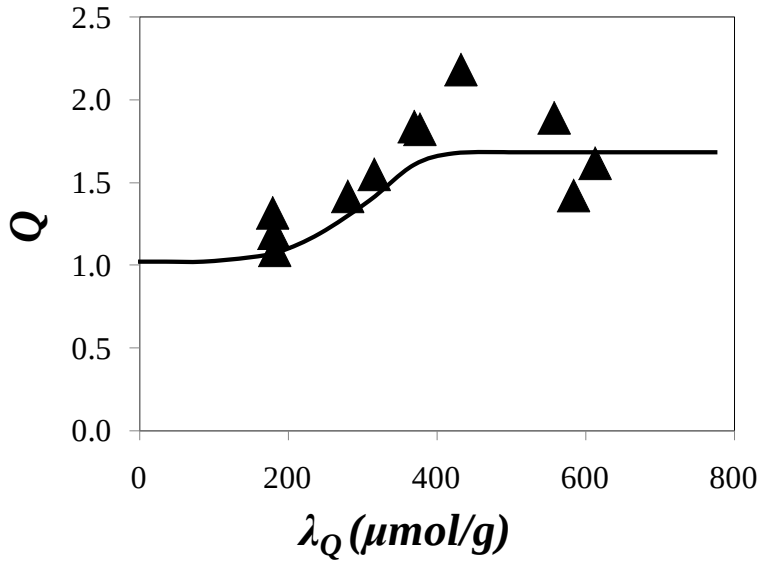

Figure 3.7. Plot of the ratio *Q* of $<\tau>_N$ of Ru-PLL over $<\tau>_N$ of Ru-PLL-Q against the quencher content.

The plot shows that the *Q* ratio is always greater than unity indicating that quenching is occurring, increasing from 1.0 to 1.8 ± 0.3 where *Q* seems to plateau for quencher contents greater than 400 μmol/g. This trend is unexpected as an increase in λ_Q results typically in a continuous increase of the *Q* ratio.

3.2. FBM Analysis of Time-Resolved Fluorescence Decays

To quantitatively describe the internal dynamics of PLL, the FBM was applied to the analysis of the Ru-PLL-Q decays. An example of the quality of fit by using Equation 2.22 is shown in Figure 3.8, where the FBM was applied to the decay of $Ru_{2.5}$-PLL-Q_{11}.

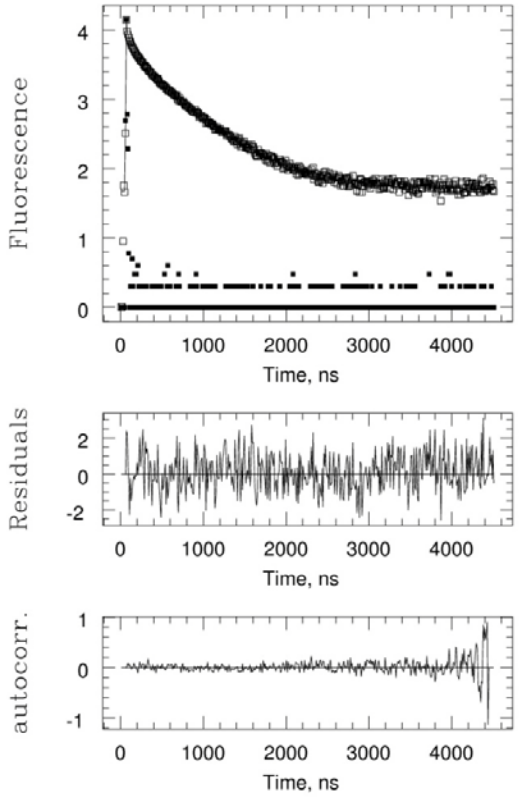

Figure 3.8. Fluorescence decay of $Ru_{2.5}$-PLL-Q_{11} in a degassed aqueous solution (λ_{ex}= 454 nm and λ_{em}= 610 nm).

It is important to mention that since the $<\tau>_N$ value of each Ru-PLL sample listed in Table 3.1A is slightly different, it needs to be taken into account to characterize the extent of quenching for each Ru-PLL-Q sample as was done in Figure 3.7. To this end, the decay times and pre-exponential factors obtained with the Ru-PLL sample used to prepare a corresponding Ru-PLL-Q sample were used to determine $F_{\mathrm{Ru}}(t)$ in Equation 2.22. The values of the parameters obtained for the fit of the Ru-PLL-Q decays with Equation 2.22 are given in Table A.3 in the Appendix. The ratio $\lambda_Q/f_{\mathrm{diff}}$ is taken as the corrected quencher content to account for the increased local concentration of quencher resulting from the existence of quencher-poor domains along the PLL backbone where Ru can not be quenched. The fraction f_{diff} represents the fraction of luminophores coming into contact with a quencher via diffusion and λ_Q is the number of moles of quencher per gram of PLL.

The size of a blob, N_{blob}, expressed in terms of the number of lysine units per blob was determined by using Equation 2.24. N_{blob} was plotted as a function of the corrected quencher content in Figure 3.9a. The N_{blob} values for PLL in aqueous solution decreased with increased quencher content. By extrapolating the N_{blob} values to zero quencher content an N^o_{blob} value of 19 ± 3 was found that corresponds to the size of an ideal blob made of PLL with no quencher. Then, k_{blob} was plotted against the corrected quencher content in Figure 3.9b. As for the N_{blob} trends, the data are scattered and our k_{blob} takes an average of $0.8 \pm 0.3 \times 10^7\ \mathrm{s}^{-1}$. The product $k_{\mathrm{blob}} \times N_{\mathrm{blob}}$ was plotted against the corrected quencher content in Figure 3.9c. As for N_{blob}, the product $k_{blob} \times N_{blob}$ decreases with increasing quencher content. After excluding the two data points shown in Figure 3.9c, $(k_{blob} \times N_{blob})^o$, the value of $k_{\mathrm{blob}} \times N_{\mathrm{blob}}$ extrapolated to zero quencher content, was found to equal $10 \pm 2 \times 10^7\ \mathrm{s}^{-1}$. These two data points were considered outliers according to the Q test.

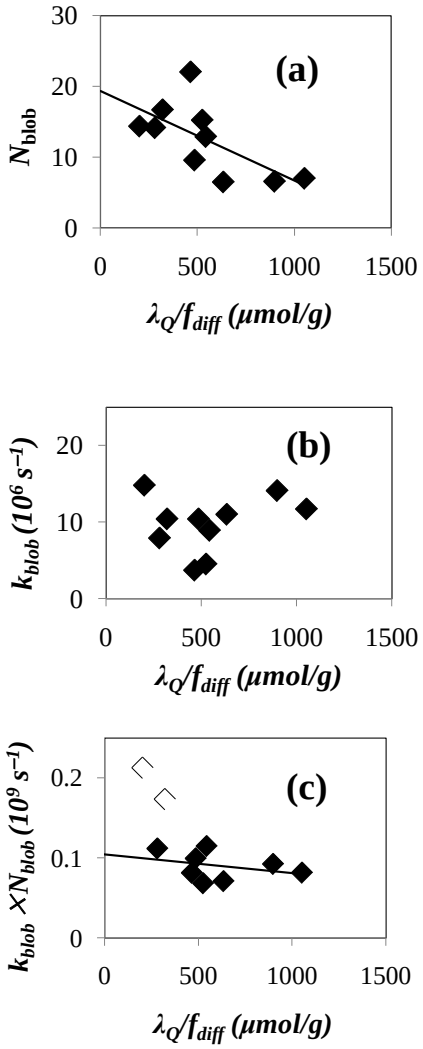

Figure 3.9. Plots of a) N_{blob}, b) k_{blob}, c) $k_{blob} \times N_{blob}$ against the corrected quencher content (λ_Q/f_{diff}).

As has been observed in earlier instances,[39] FBM analysis of fluorescence decays usually results in N_{blob} and k_{blob} trends that show a much larger extent of scatter than what is found for the product $k_{blob} \times N_{blob}$. This effect is believed to result from a cancellation of errors between k_{blob} and $\langle n \rangle$ used to determine N_{blob} whose values seem to be correlated when applying the FBM equations to the analysis of the fluorescence decays. This is a

fortunate effect, as the product $k_{blob} \times N_{blob}$ has been shown to faithfully describe the LRPCD of a number of polymers.[15,39]

The results obtained thus far indicate that the FBM can be used to fit the fluorescence decays of the Ru-PLL-Q samples in 0.01 M NaCl aqueous solution. The parameters retrieved according to the FBM analysis yielded N_{blob}^{o} and $(k_{blob} \times N_{blob})^{o}$ values of 19 ± 3 and 10 ± 2 × 10^7 s^{-1}, respectively. Together these values describe the internal dynamics of PLL, as probed by the quenching of an excited Ru by DNB covalently attached to PLL. How these internal dynamics of PLL are affected by the changes in the conformation of PLL can be investigated by applying the FBM analysis to the decays of Ru-PLL-Q solutions prepared in acidic and basic conditions to induce PLL to switch its conformation from a random-coil to an α-helix, respectively.

To this end, the time-resolved fluorescence decays of Ru-PLL and Ru-PLL-Q were obtained in 0.01 M NaCl aqueous solutions at pH 3, 5, 7, 9, 11, and 13 in order to investigate the effect of pH on the internal dynamics of Ru-PLL-Q. Ru-PLL decays were first analyzed by a sum of exponentials and $<\tau>_N$ was obtained. Decay times and their associated pre-exponential factors for all the Ru-PLL samples at pH 3, 5, 7, 9, 11, and 13 are given in Tables A.4a-f in the Appendix. These decay times and pre-exponential factors were then used to analyze the Ru-PLL-Q decays with the FBM and the parameters retrieved from this analysis are shown in Tables A.5a-f in the Appendix. The plot of N_{blob}, k_{blob}, and $k_{blob} \times N_{blob}$ versus the corrected quencher content are given in Figures 3.10a, 3.10b, and 3.10c, respectively.

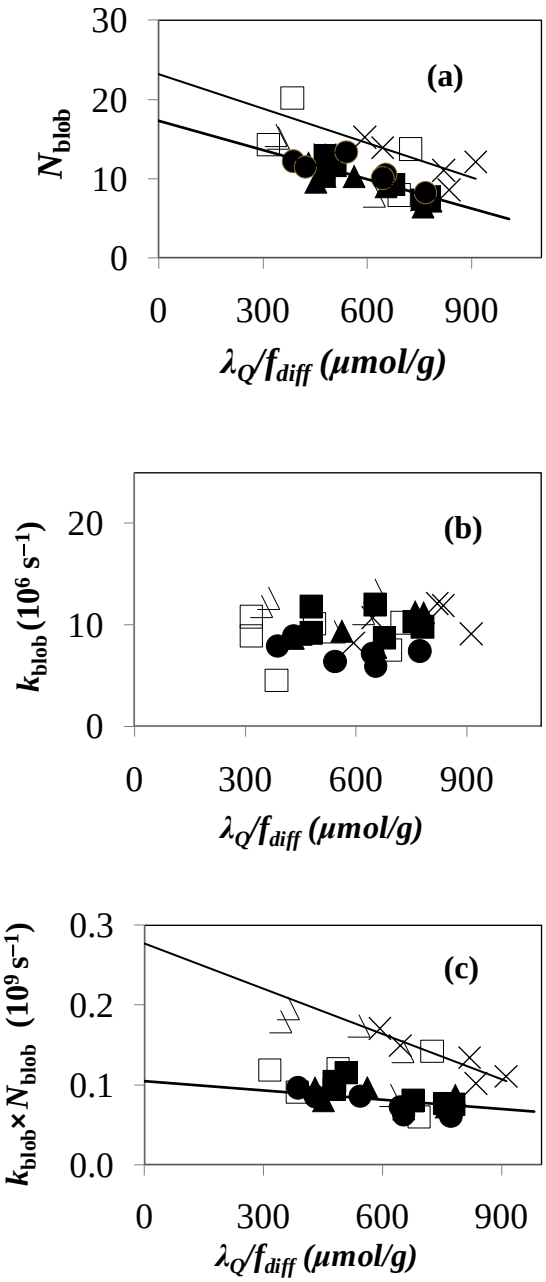

Figure 3.10. Plots of a) N_{blob}, b) k_{blob}, and c) $N_{blob} \times k_{blob}$ against the corrected quencher content (λ_Q/f_{diff}) for pH 13 (□), pH 11 (△), pH 9 (●), pH 7 (▲), pH 5 (■), pH 3 (×).

The trends obtained for the parameters k_{blob}, N_{blob}, and the product $k_{blob} \times N_{blob}$ show consistent results at pH 5, 7, and 9 where all the data points cluster around single lines. When extrapolated to zero quencher content, N^o_{blob} and $(k_{blob} \times N_{blob})^o$ values of 18 ±

1 and 10 ± 1 × 10^7 s^{-1}, respectively, were obtained at pH 5, 7, and 9. Within experimental error, these values match those obtained for PLL in 0.01 M NaCl aqueous solution and found to equal 17 ± 1 and 12 ± 1 × 10^7 s^{-1}, respectively.

At pH 3, 11, and 13, large N_{blob} values are obtained in Figure 3.10a, indicating that stronger quenching is taking place at these pH's. Whereas a stronger quenching is expected at pH 3 where the random coil conformation of PLL should result in a larger mobility of the Ru and DNB labels, this result was somewhat unexpected at pH 11 and 13 where PLL should adopt an α-helical conformation. The enhanced quenching observed at pH 11 and 13 is believed to be due to the aggregation of PLL whose solubility in water is affected by the hydrophobic DNB quencher and the data attained at these pH's will not be discussed further. At pH 3, corresponding to the more mobile random coil conformation of PLL, N_{blob}^{o} and $(k_{blob} \times N_{blob})^{o}$ values of, respectively, 23 ± 1, and 29 ± 2 × 10^7 s^{-1} were obtained.

It is important to mention that only 6 out of the 11 Ru-PLL-Q samples listed in Table 1.1B were used for the pH studies because the other samples crosslinked and were no longer soluble in water. The Ru-PLL and Ru-PLL-Q samples were found to undergo crosslinking when left in solution for too long (~ 1 month). To minimize this effect the samples which had not crosslinked yet were freeze-dried and kept at −20 °C in the dry state. The Ru-PLL-Q samples used for the pH studies together with the FBM parameters retrieved from the analysis are given in Tables A.5a-f. At pH's of 5, 7, and 9 the average number of quenchers per blob <*n*> does not increase much with increasing quencher content. Also, the fraction of Ru being quenched by diffusion, f_{diff}, does not increase with increasing quencher content. These observations suggest that increasing the quencher

content does not result in increased quenching for quencher contents larger than 5 mol%, as was observed in Figure 3.7 with the *Q* ratio. Furthermore, the fraction of unquenched luminophores, $f_{free}=1-f_{diff}$ remains unexpectedly high for all fluorescence decays.

3.3. Circular Dichroism

The changes observed in the internal dynamics of PLL in acidic (pH = 3) and basic (pHs = 5, 7, and 9) solutions were attributed to changes in the conformation of PLL. This conclusion needed to be confirmed and to this end, circular dichroism (CD) experiments were conducted. First, the CD spectra were acquired for the unlabeled PLL in milli-Q water at pH 3, 5, 7, 9, 11, and 13 (Figure 3.11a). The α-helical content (f_α) of the unlabeled PLL was determined by applying the expression given in Equation 3.4 to the CD spectra shown in Figure 3.11A.

$$f_\alpha = 1 - \frac{\theta_{222} - \theta_{RC}}{\theta_\alpha - \theta_{RC}} \qquad 3.4$$

In Equation 3.4, θ_{222} is the molar ellipticity at the wavelength of 222 nm, while θ_α and θ_{RC} are the molar ellipticities of, respectively, the α-helix and random-coil conformations at 222 nm. Implicit in the definition of f_α is that PLL adopts two states only under the conditions stated.

As mentioned earlier, PLL is expected to be in a random-coil conformation at acidic pHs and in an α-helical conformation at basic pHs. This is reflected in the CD spectra shown in Figure 3.11.

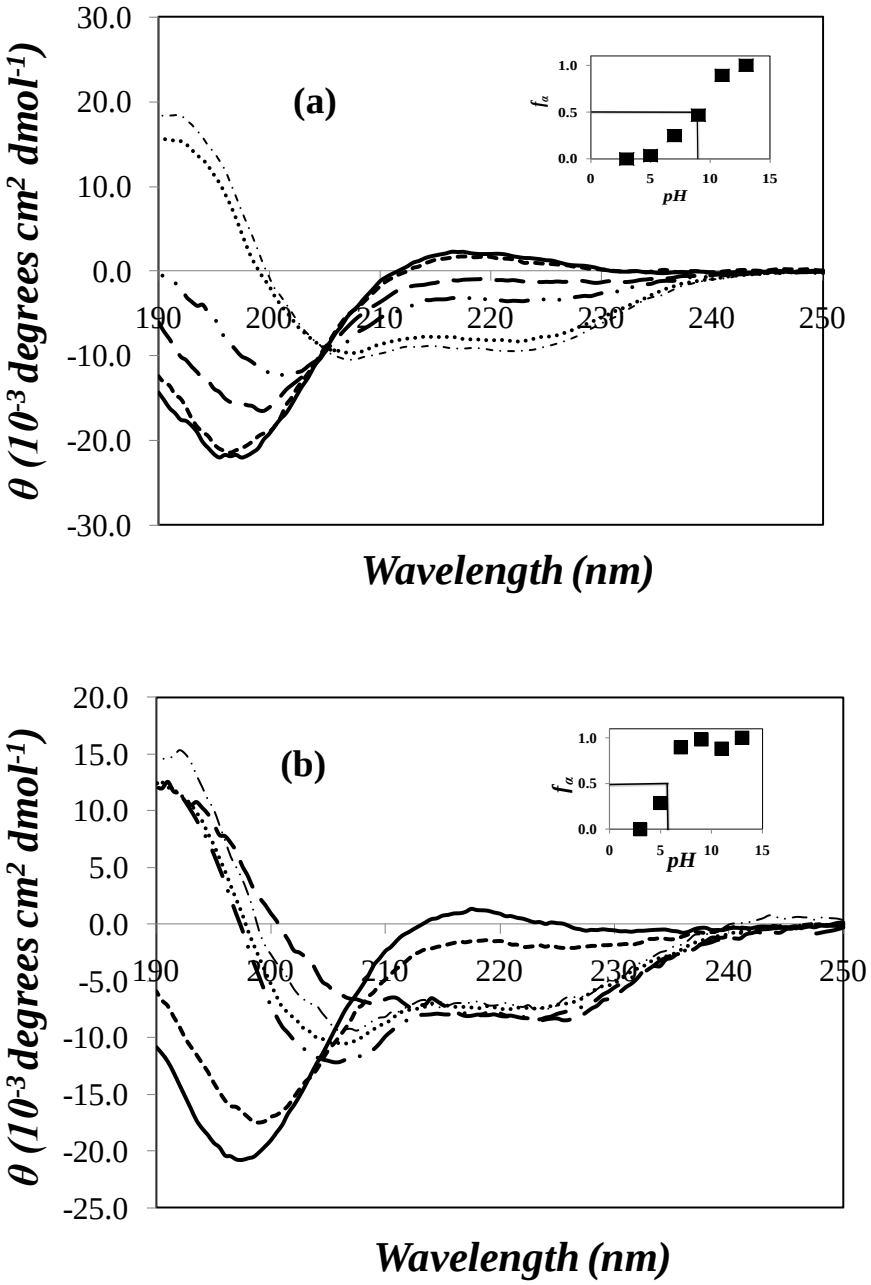

Figure 3.11. Circular dichroism spectra for a) PLL and b) $Ru_{2.6}$-PLL-Q_{11} samples in milli-Q water for pH 3 (——, pH 5 (--------), pH 7 (- - - -), pH 9 (- ·· - ·· -), pH 11 (·····), and pH 13 (-·-·-·). The insets show the α-helical content versus pH.

The CD spectra in Figure 3.11A for the unlabeled PLL in milli-Q water at pH 3 and 13 were characteristic of a random-coil and α-helical conformation, respectively, and these spectra were used to determine the values of θ_{RC} and θ_{α} in Equation 3.4. The α-helical content increased with increasing pH in the inset of Figure 3.11A.

These experiments were then repeated for the $Ru_{2.6}$-PLL-$Q_{11.0}$ samples (Figure 3.11b) in milli-Q water. The presence of the Ru and Q labels is found to shift the random coil-to-α-helix transition to lower pH values. Since the presence of 0.01 M NaCl is also expected to shift this transition to even lower pH's, the data obtained for the Ru-PLL-Q samples at pH 7 and 9 reflect the behavior of PLL adopting an α-helical conformation.

3.4. Summary of Experimental Results obtained by Fluorescence

Analysis of the fluorescence decays of the Ru-PLL-Q samples with the FBM yielded the parameters k_{blob} and N_{blob} whose product $(k_{blob} \times N_{blob})^o$ gives information about the internal dynamics of a polymer. N_{blob}^o represents the number of PLL residues found in a blob. N_{blob}^o and $(k_{blob} \times N_{blob})^o$ values for different pH's were found by extrapolating the N_{blob} and $k_{blob} \times N_{blob}$ trends to zero quencher content in Figure 3.10a and 3.10c. They are plotted in Figure 3.12 versus pH.

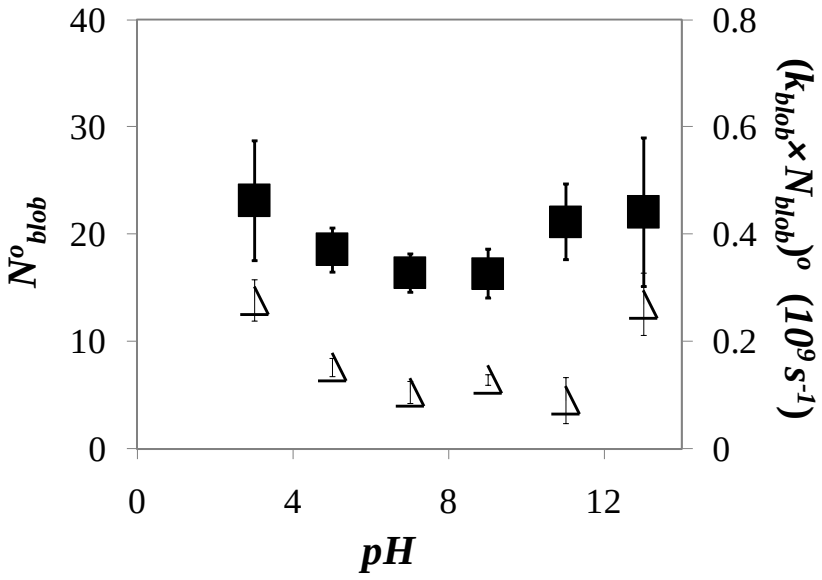

Figure 3.12. Plot of N^o_{blob} (■) and $(k_{blob} \times N_{blob})^o$ (△) a function of pH for Ru-PLL-Q samples.

N^o_{blob} decreases continuously from a value of 23 ± 6 at pH 3 to a value of 18 ± 2 at pH 9. Similarly, the product $(k_{blob} \times N_{blob})^o$ decreases with increasing pH (22 ± 0.7 × 10^7 s^{-1} at pH 3 to 15 ± 0.05 × 10^7 s^{-1} at pH 9). At pH's 11 and 13, the FBM analysis yields scattered trends, possibly due to hydrophobic aggregation of the Ru-PLL-Q samples, which makes the N^o_{blob} values at these pH's less reliable. Both N^o_{blob} and $(k_{blob} \times N_{blob})^o$ trends suggest that PLL experiences a pronounced reduction in mobility with increasing pH as could be expected if the Ru-PLL-Q constructs undergo a coil-to-helix transition. At pH 7 and 9, where the Ru-PLL-Q constructs adopt an α-helical conformation, an N^o_{blob} of 18 ± 3 is obtained, which implies that a Ru complex located at the center of a stretch of 18 lysines can reach a DNB quencher located 9 lysines up and downstream to the Ru complex. To determine whether an N^o_{blob} value of 18 ± 3 units is compatible with the geometry of an α-

helical Ru-PLL-Q construct, the modeling program Hyperchem (Hypercube, Inc) was used to find the maximum number of lysine residues between a Ru complex and a DNB quencher before Ru and DNB would fail to encounter. In turn this number would be expected to be close to $N_{blob}^{o}/2$ as other studies on pyrene-labeled poly(glutamic acid) have found.[16,17] This modeling study is based solely on geometric considerations to determine whether the Ru-complex and DNB can come into physical contact.

3.5. Molecular Mechanics Optimizations

The crystal structure of the Ru complex (RuNCS PF_6^{2-}) [40] was used to prepare the Ru-PLL-Q constructs with Hyperchem (7.02). PLL α-helices of different lengths were built using Hyperchem and the Ru complex was attached to the 8th residue of each of these constructs. For the first construct, DNB was attached to the 9th residue and the distance between the Ru complex and DNB was increased by one residue in each subsequent construct. Molecular mechanics optimizations using the Fletcher-Reeves algorithm were performed by imposing the following constraints. The distance between the Ru atom of the Ru complex and the N atom of the nitro group of DNB placed in the para position to the anilinic amine was set to equal 2.0 Å before the start of the molecular mechanics optimizations. The backbone atoms of the α-helix were held fixed in the optimization, to ensure that the construct would retain its α-helical conformation during optimization. The side chains of the PLL residues which would affect the interactions between the Ru complex and DNB were included in the optimization. After the optimization, the distance between the Ru and N atom ($d_{\text{Ru-DNB}}$) was determined. This procedure was repeated by

increasing the number of lysine residues (N_{Lys}) between the Ru complex and DNB one unit at a time from 1 to 27. Two Ru-PLL-Q constructs obtained with Hyperchem are shown in Figure 3.13.

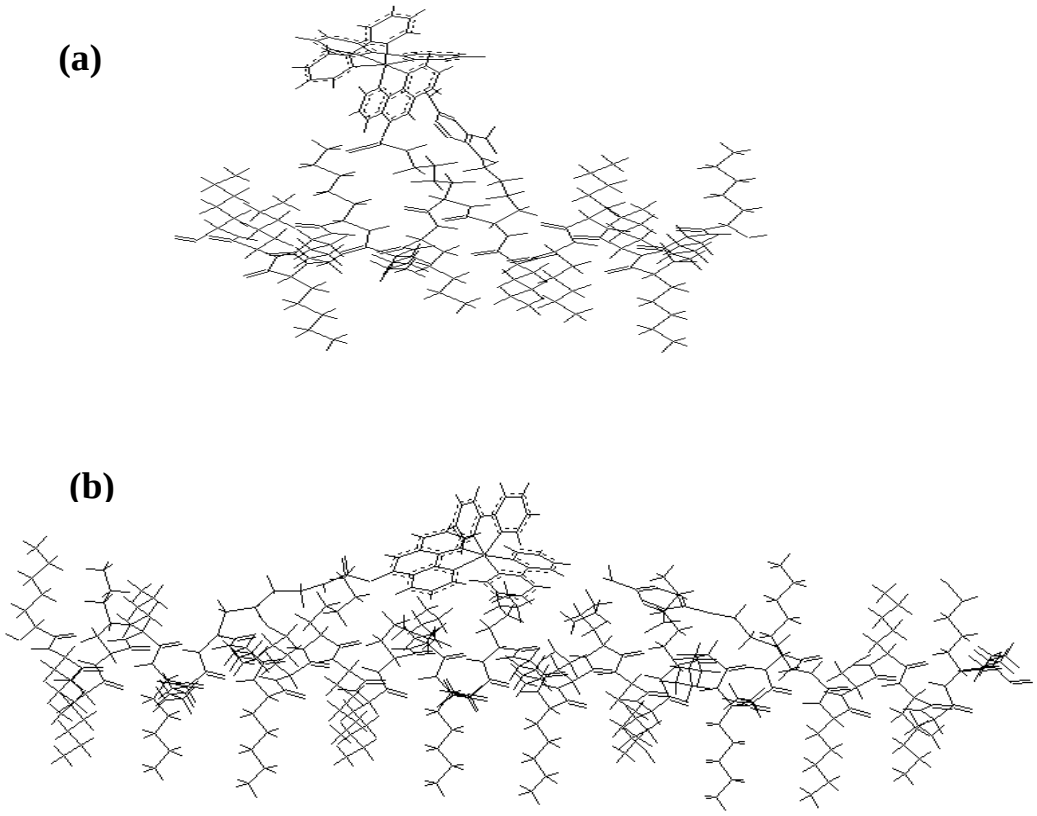

Figure 3.13. A) A Ru-PLL-Q construct bearing the Ru complex and DNB at the 8th and 9th residue, respectively, and B) the Ru complex and DNB are located at the 8th and 31st residue, respectively.

The Ru complex can encounter the DNB quencher when they are attached to nearby lysines, as in Figure 3.13a but no encounter is possible in Figure 3.13b where 22 residues separate the Ru complex from DNB. The distance of closest approach, $d_{Ru\text{-}DNB}$, is plotted against the number of lysine residues (N_{Lys}) between the Ru complex and DNB in Figure

3.14. The $d_{\text{Ru-DNB}}$ remains constant and equal to 3.8 ± 0.1 Å up to an N_{Lys} value of 16, above which $d_{\text{Ru-DNB}}$ increased linearly with N_{Lys}. The N_{Lys} value at the break point in Figure 4.3 is referred to as N_{Lys}^{o}. The plot shown in Figure 3.14 suggests that a Ru complex and DNB quencher separated by more than 16 ± 4 lysines can no longer encounter. The N_{Lys}^{o} value of 16 ± 4 lysines found by molecular mechanics optimization compares well with the N_{blob}^{o} value of 18 ± 3 lysines obtained by fluorescence. In essence, FBM analysis of the Ru-PLL-Q constructs yields the relationship $N_{Lys}^{o} \cong N_{blob}^{o}$.

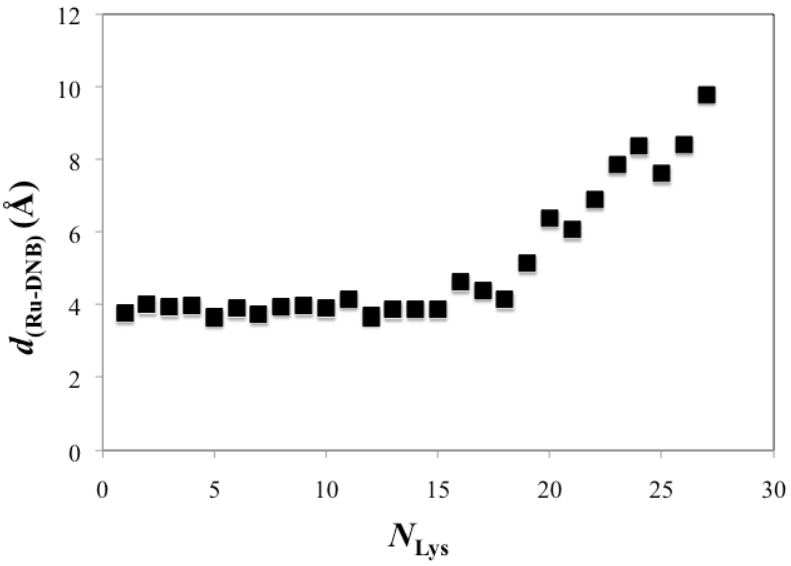

Figure 3.14. Distance of closest approach, $d_{\text{Ru-DNB}}$, as a function of the number of lysine residues, N_{Lys}, between the Ru complex attached on the 8$^{\text{th}}$ residue and DNB attached at positions 9 to 35 along a PLL α-helix.

The side-chain dynamics of an α-helical polypeptide have been characterized in an earlier study where 1-pyrenemethylamine and 1-pyrenebutylamine were attached to poly(*L*-glutamic acid) resulting in the pyrene labeled poly(*L*-glutamic acid) referred to as

PGA-PMA and PGA-PBA, respectively.[16] FBM analysis of the fluorescence decays gave N_{blob}^{o} values in DMF of 22 ± 1.5 and 31 ± 1.5 for PGA-PMA and PGA-PBA, respectively. Molecular mechanics optimizations conducted on a series of α-helical PGA-PMA and PGA-PBA constructs yielded a maximum distance of encounter between two pyrenyl pendants corresponding to a number N_{Glu}^{o} of 11 and 17 glutamic acids, respectively. An excited pyrene located at the center of a PGA blob would be expected to reach a ground-state pyrene located $N_{blob}^{o}/2$ glutamic acids upward or downward to the excited pyrene. Consequently, the N_{Glu}^{o} values obtained from molecular mechanics optimizations compared well with the $N_{blob}^{o}/2$ values obtained from fluorescence since it was found that ($N_{blob}^{o} \approx 2 \times N_{Glu}^{o} + 1$).[16] However, the relationship obtained for the Py-PGA constructs is not consistent with that found for the Ru-PLL-Q constructs and efforts were devoted into finding why that would be the case.

Since the Ru complex has a longer lifetime than the pyrenyl derivatives used in the PGA-PMA and PGA-PBA constructs, the longer-lived Ru complex is expected to probe its surroundings for a longer time so that N_{blob}^{o} for Ru-PLL-Q should be larger than that obtained for both PGA-PMA and PGA-PBA. It is thus surprising that a smaller N_{blob}^{o} of 18 ± 3 was obtained for Ru-PLL-Q in water than that of 31 ± 1.5 found for PGA-PBA in DMF.

In order to find out why N_{blob}^{o} is smaller for an α-helical PLL as compared to that of an α-helical PGA, the quenching efficiency of dinitrobenzene toward $RuNH_2$ and 1-pyrenemethanol was compared in milli-Q water with 0.01 M NaCl. To ensure that only collisional quenching would be monitored the fluorescence decays of $RuNH_2$ and 1-

pyrenemethanol were acquired and fitted with two and one exponential, respectively. The $<\tau>_N$ values were determined for each decay. The $<\tau>_N$ values obtained without DNB are reported as $<\tau>_N^o$. The ratio $<\tau>_N^o / <\tau>_N$ is plotted as a function of DNB concentration in Figure 3.15. A linear $<\tau>_N^o / <\tau>_N$ vs. [*Q*] trend demonstrates that all luminophores are equally accessible to the quencher. The Stern-Volmer plot can then be fitted with Equation 3.5, where k_q is the quenching rate constant.[37]

$$\frac{<\tau>^0_N}{<\tau>_N} = I + k_q <\tau>^0_N [Q] \qquad 3.5$$

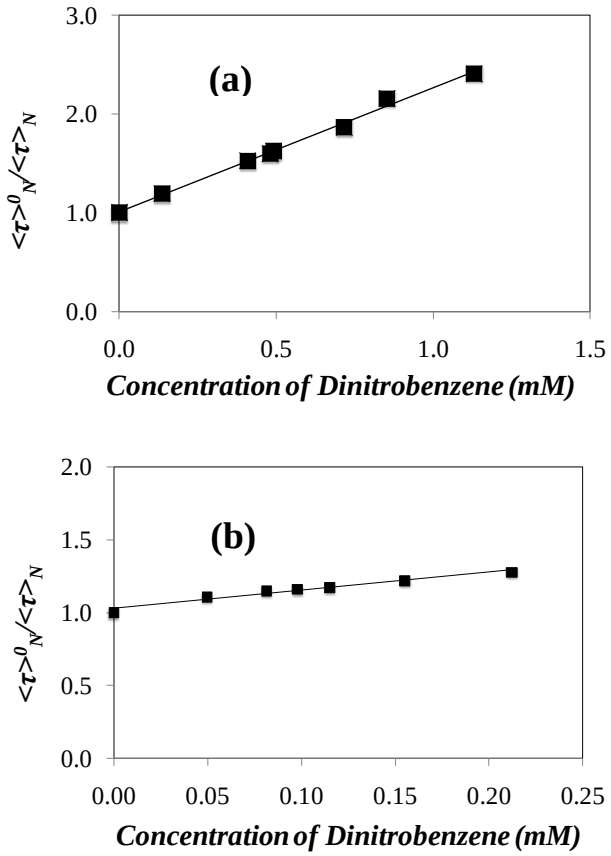

Figure 3.15. $<\tau>_N^o / <\tau>_N$ as a function of dinitrobenzene concentration in 0.01 M NaCl aqueous solution a) $RuNH_2$, b) 1-pyrenemethanol.

The Stern-Volmer plots shown in Figure 3.15a and 3.15b gave k_q values of 3.6×10^9 $M^{-1}s^{-1}$ and 1.0×10^{10} $M^{-1}s^{-1}$ for $RuNH_2$ and 1-pyrenemethanol, respectively. This result demonstrates that DNB quenches 1-pyrenemethanol better than $RuNH_2$.

The k_q value of 1.0×10^{10} $M^{-1}s^{-1}$ is the largest k_q value that can be obtained in aqueous solution. The smaller k_q value obtained for $RuNH_2$ might be a result of the large size of $RuNH_2$ (0.55 nm^3)[40] compared to that of pyrene (0.26 nm^3)[41] which hinders its diffusive motions when compared to 1-pyrenemethanol. If this were indeed the case, the bulky Ru complex would probe a smaller volume around the α-helix as reflected by the smaller N_{blob}^{o} value. However, the k_q value of 3.6×10^9 $M^{-1}s^{-1}$ for the quenching of $RuNH_2$ in water by DNB is similar to the rate constant of excimer formation found to equal to 2.10×10^9 $M^{-1}s^{-1}$ for 1-pyrenemethanol in DMF.[16] Since the FBM worked well for the PGA-PBA constructs studied in DMF, the efficient quenching of $RuNH_2$ by DNB reflected by the k_q value of 3.6×10^9 $M^{-1}s^{-1}$ suggests that the bulkiness of $RuNH_2$ cannot account for the small N_{blob}^{o} value obtained for the Ru-PLL-Q constructs.

Another parameter that affects mobility is the solution viscosity. The slightly larger viscosity of water (0.89 mPa) compared to that of DMF (0.79 mPa) would also hinder the encounter between the Ru complex and DNB attached to PLL but this effect is so small (a 13% viscosity increase) that it alone cannot account for the large difference in N_{blob}^{o} found for the Ru-PLL-Q and PGA-PBA constructs.

A blob for a PLL α-helix represents the volume of the helix that can be probed by an excited Ru attached to the PLL side chain. If the volume of a blob can be approximated to that of a cylinder, V_{blob} can be estimated as follows. The cylinder radius represents the distance separating the luminophore from the α-helical backbone and it can be determined

by using molecular mechanics optimization. A construct of $(Gly)_8$-$(Lys\text{-}Ru)_1$-$(Gly)_1$-$(Glu\text{-}PBA/PMA)_1$-$(Gly)_8$ was built in Hyperchem. The spacer between the luminophore and the polyglycine backbone was first stretched up to 50 Å and then allowed to relax, before measuring *r*, the equilibrium length of the spacer. The constructs used to determine the distances are shown in Figure 3.16.

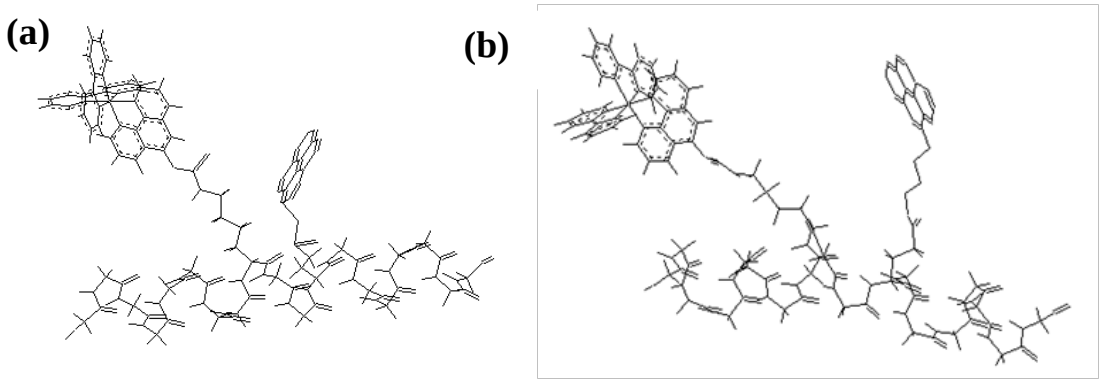

Figure 3.16. a) An α-helical construct of $(Gly)_8$-$(Lys\text{-}Ru)_1$-$(Gly)_1$-$(Glu\text{-}PMA)_1$-$(Gly)_8$, and b) $(Gly)_8$-$(Lys\text{-}Ru)_1$-$(Gly)_1$-($Glu\text{-}PBA)_1$-$(Gly)_8$.

The distance *r* between the central carbon atoms of 1-pyrenebutylamine and the backbone carbon to which it is connected (15 Å) better matched the distance between the Ru atom of the Ru complex and the backbone (15 Å) than that between the central carbon atoms of 1-pyrenemethylamine and the backbone (10 Å). Using these *r* values, $V_{\text{blob}(1)}$ for PGA-PBA and Ru-PLL-Q was estimated using Equation 3.6 in an effort to rationalize the differences found for their N_{blob}^{o} values.

$$V_{blob(1)} = \pi r^2 N_{blob} h \qquad 3.6$$

In Equation 3.6, *h* represents the increment of α-helical height per amino acid and is equal to 0.15 nm. The volumes were determined to equal 34 and 18 nm^3 for PGA-PBA and Ru-PLL-Q, respectively. According to these values, pyrene in PGA-PBA can probe almost double the volume that Ru in Ru-PLL-Q can probe. Considering that the Ru complex has a larger lifetime than the pyrene derivative, V_{blob} for the Ru complex should be larger unless its mobility is hindered due to its size. However, the quenching experiments conducted in Figures 3.15a and 3.15b suggest that this is unlikely to be the case.

Another reason which might result in a smaller N_{blob}^{o} value for the Ru-PLL-Q samples is the difference in the volumes that the Ru complex and DNB quencher can probe. Since the spacer linking DNB to the PLL backbone is smaller than that for the Ru complex, DNB may probe a smaller volume than the Ru complex. The distance *r* between the nitrogen atom of the DNB nitro group located in the position para to the anilic amine and the backbone was found to equal 11 Å using the constructs shown in Figure 3.17.

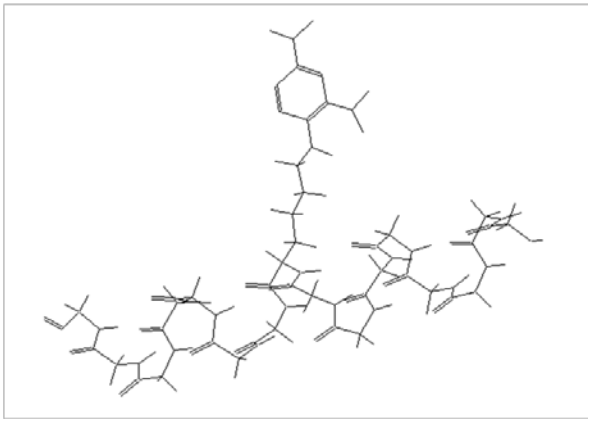

Figure 3.17. An α-helical construct of $(Gly)_8$-$(Lys\text{-}DNB)_1$-$(Gly)_8$.

Since r for DNB is substantially smaller than for the Ru complex, DNB is not expected to encounter (and quench) the Ru luminophores located more than 11 Å away from the α-helix which should result in a less efficient quenching. This proposal is described in Figure 3.18. In Figure 3.18a, a PGA-PBA α-helical chain is shown where the pyrenyl derivative PBA acts both as a luminophore and a quencher. Each PBA can extend as far as 15 Å from the PGA backbone. The N^{o}_{blob} and N^{o}_{Glu} values of 33 and 17 in Figure 3.18 are those which were those found by fluorescence and molecular mechanics, respectively. We can apply the modified version of Equation 3.6, namely Equation 3.7, to calculate V_{blob} again, where $N_{\text{polypeptide}}$ represents N^{o}_{Glu} for a PGA-PBA α-helix. A value of 36 nm^3 is obtained which is the same as that obtained by using Equation 4.2.

$$V_{blob(2)} = \pi r^2 2N_{polypeptide}\, h \qquad 3.7$$

In Figures 3.18b and 3.18 c, a PLL α-helical chain is shown with the Ru complex and quencher attached to it. The Ru complex and quencher can extend from the PLL backbone as far as 15 Å and 11 Å, respectively. The N^{o}_{blob} and N^{o}_{Lys} values of 18 and 16 in Figures 3.18b and 3.18c are those which were found by fluorescence experiments and molecular mechanics simulations, respectively.

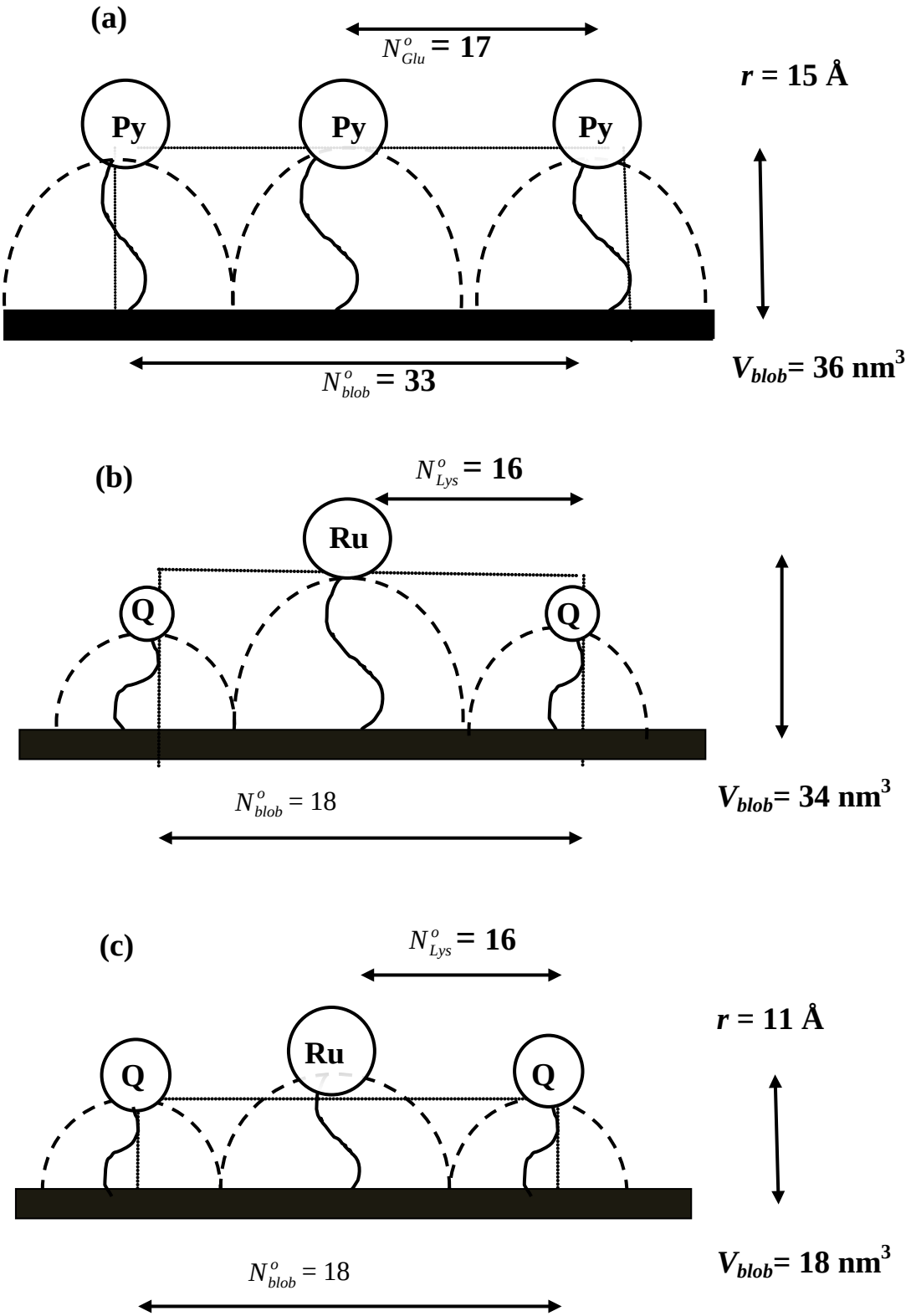

Figure 3.18. Determination of V_{blob} using Equation 4.2B for a) PGA-PBA, and Ru-PLL-Q chains by assuming b) r = 15 Å, and c) r = 11 Å.

In Figures 3.18b and 3.18c, V_{blob} is calculated by making two assumptions. In the first assumption, r is taken to equal 15 Å (Figure 3.18b) in Equation 3.7 and a V_{blob} value of 36 nm^3 is obtained, close to that of 34 nm^3 obtained for a PGA-PBA α-helix. In the second assumption, an r value of 11 Å instead of 15 Å is taken in Equation 3.7 (Figure 4.18c), and a value of 18 nm^3 is calculated for V_{blob} which is same as the one that was obtained for Ru-PLL-Q using Equation 3.6 (44 nm^3). In other words, if DNB were also able to extend as far as the Ru complex does (15 Å), then V_{blob} would be equal to 36 nm^3. But since DNB can only reach up to 11 Å, it can only probe a V_{blob} of 18 nm^3. If DNB is unable to probe the same volume as the Ru complex, quenching of Ru would be expected to be less efficient resulting in the large f_{free} values listed in the Table A.5d and e, a small number of quenchers would be able to saturate the small volume as shown in Figure 3.18, and no further change in the fluorescence decays would be observed. Furthermore, these considerations could also suggest that the limiting factor to consider when doing quenching experiments is the smaller volume probed by the quencher and the luminophore. If proven correct, such considerations could be of tremendous importance when designing quenching experiments.

One more reason which could explain the smaller N^{o}_{blob} value obtained for the Ru-PLL-Q construct is the hydrophobicity of the DNB quencher. While the water solubility of FDNB equals 8.6 mM at 17 °C, it is possible that the Ru-PLL-Q constructs with a larger DNB content could cause the quencher to aggregate intra- or intermolcularly. This rationale is suggested by Figure 3.7, where the ratio Q of $<\tau>_N$ of Ru-PLL over $<\tau>_N$ of Ru-PLL-Q does not increase with increasing quencher content larger than ~5 mol%. Furthermore, degassing the Ru-PLL-Q samples with nitrogen resulted in bubbling which

demonstrates the ampiphillic character of the labeled PLL constructs and provides an indirect evidence of aggregation.

4. Conclusions and Future Work

4.1. Conclusions

This study represents the first attempt to apply the FBM to study the internal dynamics of a polymer in aqueous solution. A polypeptide (PLL) was randomly labeled with a ruthenium complex as a luminophore and FDNB as a quencher. The ruthenium complex $RuNH_2$ was successfully synthesized and characterized. It was then converted to RuNCS to allow its attachment onto PLL via a thiourea linkage. PLL was first labeled with RuNCS to obtain the Ru-PLL samples. These samples were characterized and further reacted with FDNB to obtain the Ru-PLL-Q samples.

The fluorescence decays of the Ru-PLL samples were obtained before and after the quencher attachment and quenching was observed. The series of decays acquired for the Ru-PLL-Q samples were then analyzed with the FBM by using the decay times and pre-exponential factors of the corresponding Ru-PLL samples. These Ru-PLL-Q samples were first studied in milli-Q water and the FBM parameters N_{blob} and $N_{\mathrm{blob}} \times k_{\mathrm{blob}}$ were plotted against the corrected quencher content and extrapolated to zero quencher content to get the N_{blob}^{o} and $(k_{blob} \times N_{blob})^{o}$ values of 19 ± 3 and 10 ± 2 x 10^7 s^{-1}, respectively. Then, these Ru-PLL-Q samples were studied in a set of acidic and basic solutions to determine whether they would be affected by a conformational change of PLL. The $N_{\mathrm{blob}} \times k_{\mathrm{blob}}$ values were clustered for pH's 5, 7, and 9, while at pH 3, 11, and 13, they were scattered and took large

values. It was concluded that the higher N_{blob}^{o} and $(k_{blob} \times N_{blob})^{o}$ values obtained at pH 3 were due to the random-coil conformation of the PLL backbone, while at pH's of 11 and 13, the possible aggregation of hydrophobic quenchers might have resulted in high N_{blob}^{o} and $(k_{blob} \times N_{blob})^{o}$ values. The N_{blob}^{o} and $(k_{blob} \times N_{blob})^{o}$ values of 17 ± 2 and 12 ± 1 × 10^{7} s^{-1} obtained at, respectively, pH 7 and 9 agreed with those obtained from the fluorescence data of Ru-PLL-Q in water.

The CD spectra for the unlabeled PLL and the Ru-PLL-Q samples were obtained at the same pH's as those used for fluorescence to compare the CD results with those obtained from fluorescence. The unlabeled PLL was a random-coil at pH 3 and with an increase in pH, the α-helical content was found to increase. The transition from a random-coil to an α-helix occurred at pH 9, while for the Ru-PLL-Q sample, the transition from the random-coil to an α-helix shifted to a lower pH of 6. Comparing these CD results with the fluorescence data, it was concluded that Ru-PLL-Q is in a random-coil conformation at pH 3 and in an α-helical conformation at pH 7 and 9. This observation explained why the $(k_{blob} \times N_{blob})^{o}$ values were higher at pH 3 and similar for pH's 7 and 9. It is believed that for pH's 11 and 13 hydrophobic interactions between the DNB quenchers led to aggregation of the Ru-PLL-Q constructs which also gave skewed results for the $(k_{blob} \times N_{blob})^{o}$ product.

In order to check if an N_{blob}^{o} of 18 was compatible with the geometry of Ru-PLL-Q, molecular mechanics optimizations were carried out using the Fletcher-Reeves algorithm with the Hyperchem software (Hypercube, Inc). This software was used to find the maximum number of lysine residues between a Ru complex and a DNB quencher before

Ru and DNB would fail to encounter. Ru-PLL-Q constructs were built by attaching the Ru complex and DNB on the side chains of a PLL α-helix. The distance between the Ru complex and DNB was increased by one lysine unit in each subsequent construct and the distance between the Ru atom of the Ru complex and the N atom of the para nitro group of DNB ($d_{\text{Ru-DNB}}$) was determined. This distance, $d_{\text{Ru-DNB}}$, was plotted against the number of lysine residues (N_{Lys}) between the Ru complex and DNB and it was found that a Ru complex and DNB quencher separated by more than 16 ± 4 lysines could no longer encounter. The N^o_{Lys} value of 16 ± 4 lysines found by molecular mechanics optimization compared well with the N^o_{blob} value of 18 ± 3 lysines obtained by fluorescence.

The N^o_{blob} value of 18 ± 3 found in this study was compared to an earlier study where N^o_{blob} values of 22 ± 1.5 and 31 ± 1.5 were found by fluorescence for PGA-PMA and PGA-PBA,[16] respectively. Thus, the N^o_{blob} value of 18 ± 3 of an α-helical PLL was smaller than those obtained for the α-helical PGA constructs, even though the Ru complex is longer-lived than the two pyrenyl derivatives used in the PGA study. Furthermore, in the PGA study, the N^o_{Glu} values obtained from the molecular mechanics optimizations were about half of those obtained for N^o_{blob} by fluorescence. This result led to the conclusion that a PGA blob with an excited pyrene at its center would reach a ground-state pyrene located $N^o_{blob}/2$ glutamic acids upward or downward, a result that contradicts the finding of the current study that a Ru complex located at the center of a stretch of 18 ± 3 lysines can reach a DNB quencher located ~ 18 lysines up and downstream to the Ru complex. As was determined by molecular mechanics optimizations, an N^o_{Lys} value of 16 ± 4 was obtained which is not half of N^o_{blob}.

The possible reasons for the difference in the N_{blob}^{o} values could be the difference in the quenching rate constants of the quencher DNB for Ru and pyrene, the volumes Ru-PLL and Q-PLL can probe, and the viscosities of the solvents used for these studies. The quenching efficiency of DNB for $RuNH_2$ and 1-pyrenemethanol was estimated by determining the quenching rate constants found to equal 3.6×10^9 and 1.0×10^{10} $M^{-1}s^{-1}$ for $RuNH_2$ and 1-pyrenemethanol in water, respectively. The quenching rate constant of 3.6×10^9 $M^{-1}s^{-1}$ for $RuNH_2$ shows that DNB quenches $RuNH_2$ efficiently so that poor quenching of Ru by DNB cannot account for the smaller N_{blob}^{o} value obtained by fluorescence. The volumes probed by the pyrene label of PGA-PBA and the quencher of Ru-PLL-Q, V_{blob}, were determined by molecular mechanics optimizations and were found to equal 34 and 18 nm^3, respectively. The difference in these two volumes suggests that DNB cannot reach out as far as the Ru complex so that not all the Ru luminophores can be quenched by the DNB quencher. Indeed V_{blob} for Ru-PLL-Q would have been 34 nm^3 if DNB could have reached as far as the Ru complex. The difference in the probing volumes of the Ru complex and DNB is suspected to result in the poor quenching of Ru by DNB and hence, smaller V_{blob} and N_{blob}^{o} values.

4.2. Future Work

In order to check if the hydrophobicity of the DNB quencher is responsible for the smaller N_{blob}^{o} value obtained in this study, the fluorescence experiments will be repeated in a 1:2 mixture of milli-Q water and ethanol. This water/ethanol mixture was used to label the PLL with the DNB quencher and DNB should be fully soluble in this mixture and thus it should prevent the aggregation of the Ru-PLL-Q chains, especially at higher pH's. Also, if

the length of the spacer linking the quencher to the PLL backbone turns out to be the major reason for the smaller N_{blob}^{o} value obtained in the current study, the whole study could be repeated using an extended linker, for example, by intercalating glycine between the quencher and the PLL backbone. This extended linker would allow the quencher DNB to probe the same volume as the Ru complex and hence enhance the quenching efficiency of DNB. These new constructs would result in a larger N_{blob}^{o} value than the one obtained in the current study.

References

1. Eaton, W. A.; Munoz, V.; Hagen, S. J.; Jas, G. S.; Lapidus, L. J.; Henry, E.R.; Hofrichter, J. *Annu. Rev. Biophys. Biomol. Struct*. **2000**, *29*, 327-359.
2. Siu, H.; Duhamel, J. *Macromolecules* **2005**, *38*, 7184-7186.
3. Pilar, J.; Labsky, J. In *Advanced ESR Methods in Polymer Research Ed*. Schlick, S., Wiley-Interscience NJ, **2006**.
4. Daragan, V.A.; Mayo, K.H. *Prog. Nuclear Magn. Resonance Spec*. **1997**, *31*, 63-105.
5. Viovy, J.-L.; Monnerie, L. *Adv. Polym. Sci*. **1985**, *67*, 99-122.
6. Valeur, B.; Jarry, J.-P.; Geny, F.; Monnerie, L. *J. Polym. Sci.: Polym. Phys. Ed*. **1975**, *13*, 667-674.
7. Winnik, M. A. *Acc. Chem. Res*. **1985**, *18*, 73-79.
8. Cuniberti, C.; Perico, A. *Eur. Polym. J*. **1977**, *13*, 369-374.
9. Kane, M. A.; Panudey, S.; Baker, G. A.; Perez, S. A.; Bukowski, E. J.; Hoth, D. C.; Bright, F. V. *Macromolecules* **2001**, *34*, 6831-6838.
10. Wilemski, G.; Fixman, M. *J. Chem. Phys*. **1974**, *60*, 866-877.
11. Ingratta, M.; Hollinger, J.; Duhamel, J. *J. Am. Chem. Soc.* **2008**, *130*, 9420-9428.
12. Mathew, A. K.; Siu, H.; Duhamel, J. *Macromolecules* **1999**, *32*, 7100–7108.
13. Duhamel, J. *Acc. Chem. Res*. **2006**, *39*, 953-960.
14. Kanagalingam, S.; Spartalis, J.; Cao, T.-C.; Duhamel, J. *Macromolecules* **2002**, *35*, 8571-8577.
15. Teertstra, S. J.; Lin, W. Y.; Gauthier, M.; Ingratta, M.; Duhamel, J. *Polymer* **2009**, *50*, 5456-5466.
16. Ingratta, M.; Duhamel, J. *J. Phys. Chem. B* **2008**, *112*, 9209-9218.

17. Duhamel, J.; Kanagalingam, S.; O'Brien, J.T.; Ingratta, M. *J. Am. Chem. Soc*. **2003**, *125*, 12810-12822.

18. Siu, H.; Duhamel, J. *Macromolecules* **2006**, *39*, 1144-1155.

19. Campagna, S.; Puntoriero, F.; Nastasi, F.; Bergamini, G.; Balzani, V. *Top. Curr. Chem.* **2007**, *280*, 117-214.

20. Friedman, A. E.; Chambron, J. C.; Sauvage, J. P.; Turro, N. J.; Barton, J. K. *J. Am. Chem. Soc.* **1990**, *112*, 4960–4962.

21. Malins, C.; Glever, H. G.; Keyes, T. E.; Vos, J. G.; Dressick, W. J.; MacCraith, B. D. *Sensors and Actuators B: Chem.* **2000**, *67*, 89-95.

22. Rudmann, H.; Shimada, S.; Rubner, M. F. *J. Am. Chem. Soc*. **2002**, *124*, 4918–4921.

23. Demas, J. N.; DeGraff, B. A. *Topics in Luminescence Spectroscopy, Volume 4: Probe Design and Chemical Sensing*, ed. J.R. Lakowicz, Plenum Press, New York, **1994**.

24. Juris, A.; Balzani, V.; Barigelletti, F.; Campagna, S.; Belser, P.; Von Zelewsky, A. *Coordination Chem. Rev.* **1988**, *84*, 85–277.

25. Anfinsen, C. B. *Advances in Protein Chemistry*, Volume 13, Academic Press, New York, **1958**.

26. Sanger, F. *Biochem. J*. **1945**, *39*, 507-515.

27. Murdock, A. L.; Grist, K. L.; Hirs, C. H. W. *Arch. Biochem. Biophys*. **1966**, *114*, 375-390.

28. Yekta, A.; Xu, B.; Duhamel, J.; Adiwidjaja, H.; Winnik, M. A. *Macromolecules* **1995**, *28*, 956-966.

29. Branden, C.; Tooze, J. *Introduction to Protein Structure,* Garland Publishing, **1998**.

30. Chittchang, M.; Miller, N.; Alur, H. H.; Velde, D. J. V.; Mitra, M. K.; Johnston, T. P. *J. Pharm. Pharmacol*. **2002**, *54*, 1497.

31. Muller, M.; Buchet, R.; Fringeli, U.P. *J. Phys. Chem*. **1996**, *100*, 10810.

32. Greenfield, N.; Fasman, G. D. *Biochemistry* **1969**, *8*, 4108-4116.

33. Ellis, C. D.; Margerum, L. D.; Murray, R. W.; Meyer, T. J. *Inorg. Chem.* **1983**, *22*, 1283–1291.

34. Quinn, C. Master's Thesis, University of Waterloo, Waterloo, 2007.

35. Ryan, E.; O'Kennedy, R.; Feeney, M. M.; Kelly, J. M.; Vos, J. G. *Bioconjugate Chem.* **1992**, *3*, 285–290.

36. Brooks, J. L.; Lucas, F.; Shaw, T. B.; Smith, S. G. *Anal. Biochem*. **1963**, *6*, 335-351.

37. Lakowicz, J. R. *Principles of Fluorescence Spectroscopy, 2*[nd] *Ed*. Kluwer
38. Academic/Plenum Publishers: New York, **1999**.

39. Lucas, F.; Shaw, T. B.; Smith, S. G. *Anal. Biochem*. **1963**, *6*, 335-351.

40. Ingratta, M.; Mathew, M.; Duhamel, J. *Can. J. Chem.* **2010**, *88*, 217-227.

41. Nag, S.; Pal, A. K.; Hanan, G. S. *Acta Cryst*. **2009**, *E65*, m1184.

42. Roberston, J. M.; White, J. *J. Chem. Soc.* **1947**, 358-368

Appendix A

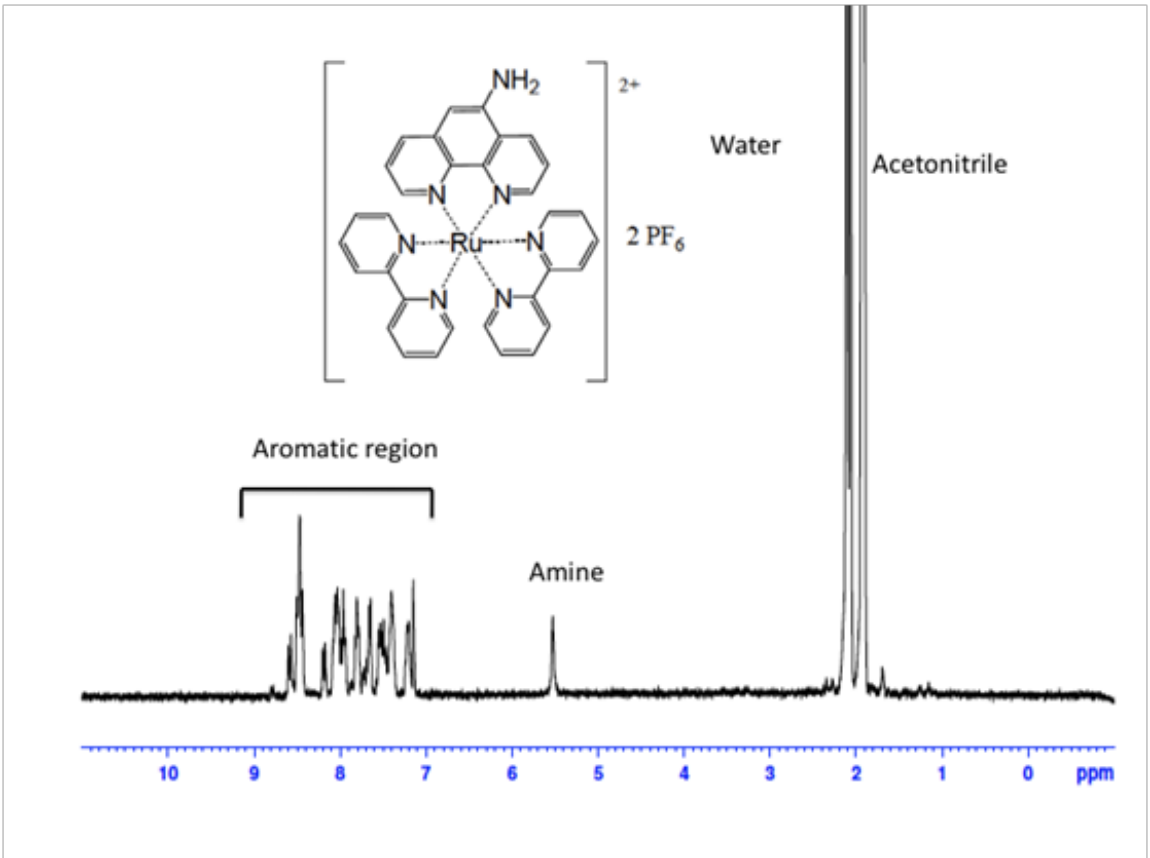

Figure A.1. ^{1}H NMR spectrum of $RuNH_2$ in acetonitrile.

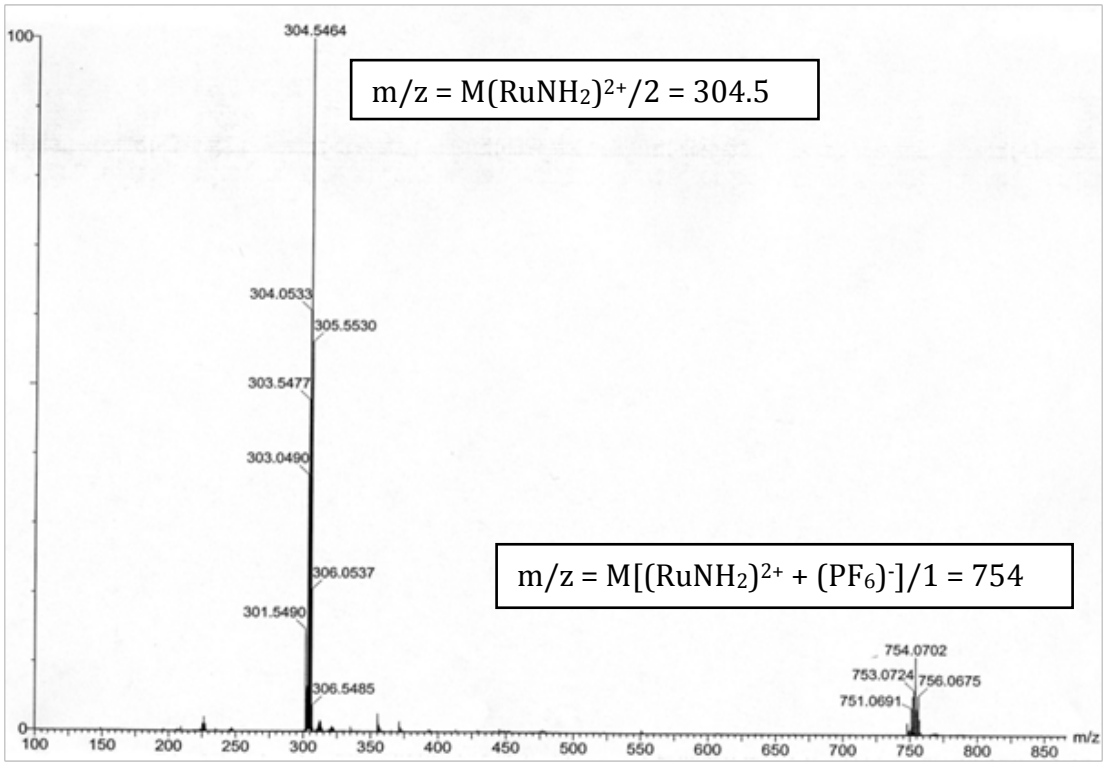

Figure A.2. Mass spectrum of $RuNH_2$ in a 1:1 acetone:water mixture.

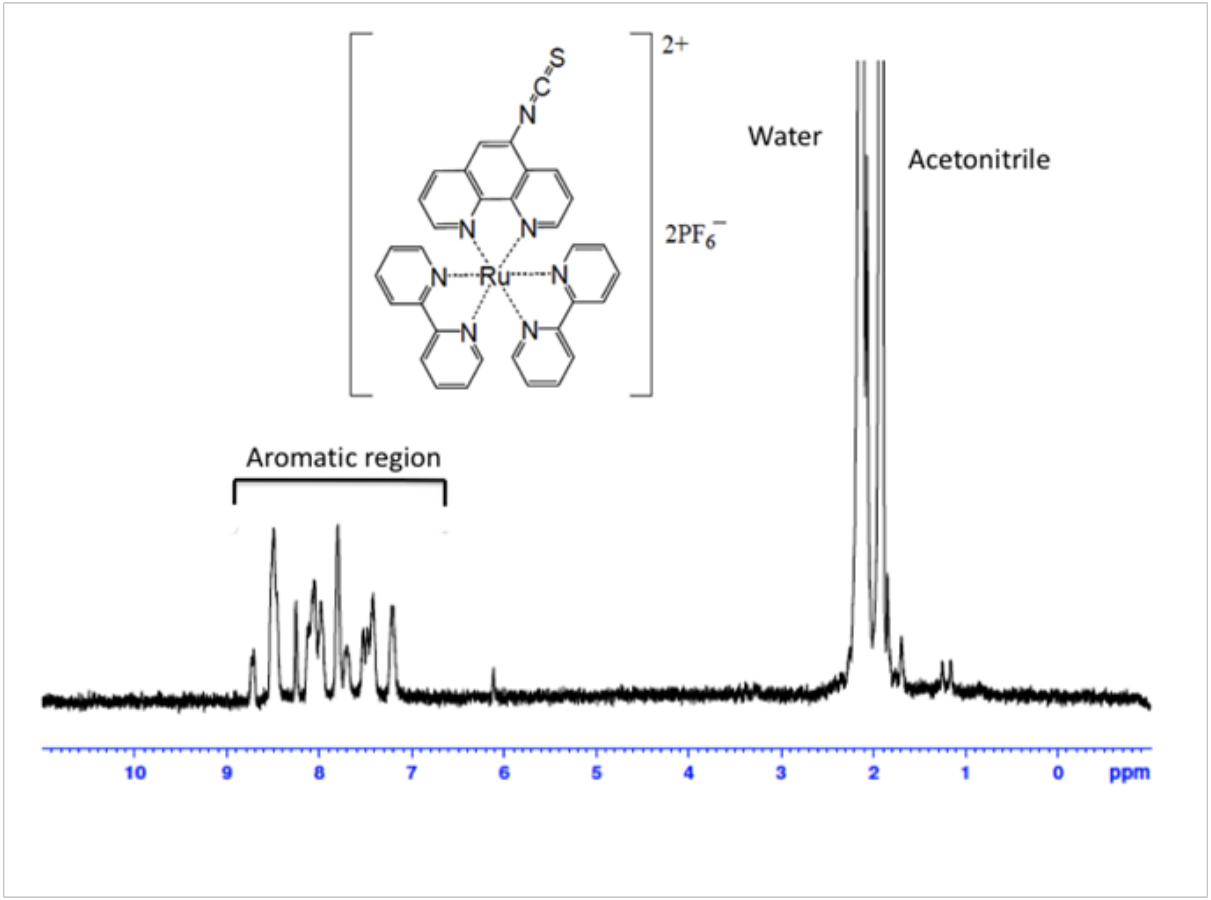

Figure A.3. ^{1}H NMR spectrum of RuNCS in acetonitrile.

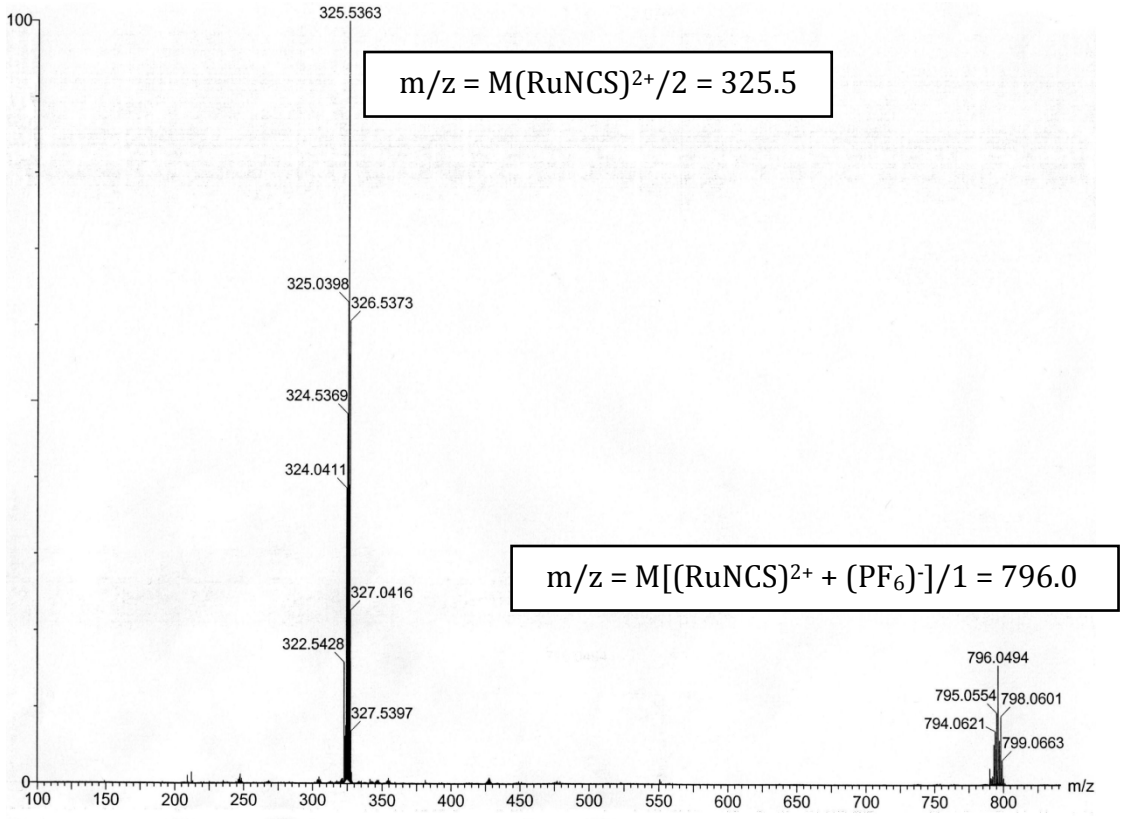

Figure A.4. Mass spectrum of RuNCS in a 1:1 acetone:water mixture.

Table A.1. Pre-exponential factors and decay times obtained from the fit of the fluorescence decays of the Ru-PLL samples in water with Equation 2.21.

Sample	τ_1	a_1	τ_2	a_2	τ_3	a_3	$\langle\tau\rangle_N$	χ^2
$Ru_{0.6}$-PLL			389	0.22	877	0.78	767	1.2
$Ru_{2.5}$-PLL			484	0.12	1392	0.88	1283	0.9
$Ru_{1.5}$-PLL			314	0.09	940	0.91	883	1.1
$Ru_{0.9}$-PLL			260	0.27	773	0.73	635	1.1
$Ru_{2.0}$-PLL	190	0.13	491	0.56	849	0.30	559	1.1
$Ru_{1.2}$-PLL			283	0.20	791	0.80	689	1.2
$Ru_{1.0}$-PLL			369	0.44	756	0.56	586	1.2
$Ru_{1.6}$-PLL			401	0.42	778	0.58	619	1.2
$Ru_{2.6}$-PLL	163	0.17	434	0.59	818	0.23	478	1.1
$Ru_{2.2}$-PLL	100	0.05	346	0.49	783	0.45	577	1.1
$Ru_{2.1}$-PLL	132	0.07	438	0.58	784	0.35	535	1.1

Table A.2. Pre-exponential factors and decay times obtained from the fit of the fluorescence decays of the Ru-PLL-Q samples in water with Equation 2.21.

Sample	τ_1	a_1	τ_2	a_2	τ_3	a_3	$\langle\tau\rangle_N$	χ^2
$Ru_{0.6}$-PLL-$Q_{2.7}$	46	0.24	307	0.19	901	0.57	583	1.1
$Ru_{2.5}$-PLL-$Q_{3.3}$			248	0.23	1323	0.77	1075	1.1
$Ru_{1.5}$-PLL-$Q_{3.4}$			293	0.3	1033	0.77	811	1.1
$Ru_{0.9}$-PLL-$Q_{4.9}$			175	0.55	698	0.45	410	1.1
$Ru_{2.0}$-PLL-$Q_{5.3}$			197	0.63	728	0.37	395	1.2
$Ru_{1.2}$-PLL-$Q_{5.9}$	65	0.29	315	0.38	728	0.33	378	1.2
$Ru_{1.0}$-PLL-$Q_{7.1}$			137	0.63	630	0.37	319	1.1
$Ru_{1.6}$-PLL-$Q_{8.4}$			146	0.69	586	0.31	284	1.2
$Ru_{2.6}$-PLL-$Q_{11.0}$	46	0.47	248	0.33	747	0.20	253	0.9
$Ru_{2.2}$-PLL-$Q_{11.5}$			165	0.52	670	0.478	406	1.1
$Ru_{2.1}$-PLL-$Q_{12.1}$			175	0.68	665	0.32	331	1.2

Table A.3. FBM parameters retrieved by using Equation 2.22 for the analysis of the fluorescence decays of the Ru-PLL-Q samples in water.

Sample	$\langle n \rangle$	f_{diff}	f_{free}	$k_{blob}(10^6\ s^{-1})$	$k_{exch}(10^6\ s^{-1})$	N_{blob}	χ^2
$Ru_{0.6}$-PLL-$Q_{2.7}$	0.44	0.88	0.11	0.014	7.0	14.36	1.13
$Ru_{2.5}$-PLL-$Q_{3.3}$	1.07	0.56	0.44	0.010	4.0	16.67	0.94
$Ru_{1.5}$-PLL-$Q_{3.4}$	0.64	0.78	0.22	0.008	1.5	17.10	1.17
$Ru_{0.9}$-PLL-$Q_{4.9}$	0.74	0.64	0.35	0.010	1.5	9.55	1.04
$Ru_{2.0}$-PLL-$Q_{5.3}$	2.06	0.60	0.40	0.004	1.4	22.02	1.05
$Ru_{1.2}$-PLL-$Q_{5.9}$	1.15	0.69	0.31	0.009	1.6	12.87	1.02
$Ru_{1.0}$-PLL-$Q_{7.1}$	1.32	0.74	0.26	0.025	1.7	13.57	1.10
$Ru_{1.6}$-PLL-$Q_{8.4}$	1.62	0.82	0.18	0.004	1.0	15.21	1.20
$Ru_{2.6}$-PLL-$Q_{11.0}$	0.88	0.87	0.13	0.011	2.8	6.46	0.96
$Ru_{2.2}$-PLL-$Q_{11.5}$	1.89	0.53	0.47	0.007	2.4	8.14	1.12
$Ru_{2.1}$-PLL-$Q_{12.1}$	1.39	0.68	0.3149	0.012	4.3	7.29	1.04

Table A.4a. Pre-exponential factors and decay times obtained from the fit of the fluorescence decays of the Ru-PLL samples in 0.01M NaCl aqueous solution at pH 3 with Equation 2.21.

Sample	τ_1	a_1	τ_2	a_2	τ_3	a_3	$\langle\tau\rangle_N$	χ^2
$Ru_{1.0}$-PLL			433	0.39	805	0.61	658	1.13
$Ru_{1.6}$-PLL			456	0.35	828	0.65	692	1.05
$Ru_{2.6}$-PLL	188	0.04	450	0.49	728	0.47	570	1.05
$Ru_{2.2}$-PLL	24	0.02	379	0.27	769	0.7	641.	0.91
$Ru_{2.1}$-PLL	271	0.08	715	0.40	989	0.51	818	1.08

Table A.4b Pre-exponential factors and decay times obtained from the fit of the fluorescence decays of the Ru-PLL samples in 0.01M NaCl aqueous solution at pH 5 with Equation 2.21.

Sample	τ_1	a_1	τ_2	a_2	τ_3	a_3	$\langle\tau\rangle_N$	χ^2
$Ru_{2.0}$-PLL			230	0.13	557	0.88	520	1.05
$Ru_{1.0}$-PLL			254	0.19	615	0.81	546	1.11
$Ru_{1.6}$-PLL			417	0.38	760	0.62	629	0.97
$Ru_{2.6}$-PLL	304	0.15	502	0.49	664	0.36	530	0.98
$Ru_{2.2}$-PLL	154	0.06	495	0.61	759	0.33	561	1.02
$Ru_{2.1}$-PLL	275	0.15	599	0.51	925	0.35	664	1.04

Table A.4c. Pre-exponential factors and decay times obtained from the fit of the fluorescence decays of the Ru-PLL samples in 0.01M NaCl aqueous solution at pH 7 with Equation 2.21.

Sample	τ_1	a_1	τ_2	a_2	τ_3	a_3	$\langle\tau\rangle_N$	χ^2
$Ru_{2.0}$-PLL	33	0.04	309	0.23	630	0.73	532	1.02
$Ru_{1.0}$-PLL			266	0.36	624	0.64	495	1.06
$Ru_{1.6}$-PLL	61	0.06	379	0.34	608	0.6	497	1.08
$Ru_{2.6}$-PLL	99	0.051	404	0.39	670	0.56	537	0.99
$Ru_{2.2}$-PLL	110	0.07	380	0.41	582	0.52	466	1.12
$Ru_{2.1}$-PLL	104	0.07	435	0.66	685	0.26	476	1.08

Table A.4d. Pre-exponential factors and decay times obtained from the fit of the fluorescence decays of the Ru-PLL samples in 0.01M NaCl aqueous solution at pH 9 with Equation 2.21.

Sample	τ_1	a_1	τ_2	a_2	τ_3	a_3	$\langle\tau\rangle_N$	χ^2
$Ru_{2.0}$-PLL	60	0.06	306	0.23	673	0.72	558	1.07
$Ru_{1.0}$-PLL			192	0.41	650	0.59	462	1.09
$Ru_{1.6}$-PLL	68	0.06	339	0.44	663	0.5	484	0.98
$Ru_{2.6}$-PLL	45	0.07	334	0.26	690	0.68	559	0.96
$Ru_{2.2}$-PLL			230	0.38	690	0.62	515	1.09
$Ru_{2.1}$-PLL	78	0.08	350	0.73	772	0.18	403	1.00

Table A.4e. Pre-exponential factors and decay times obtained from the fit of the fluorescence decays of the Ru-PLL samples in 0.01M NaCl aqueous solution at pH 11 with Equation 2.21.

Sample	τ_1	a_1	τ_2	a_2	τ_3	a_3	$\langle\tau\rangle_N$	χ^2
$Ru_{2.0}$-PLL	79	0.13	409	0.21	709	0.66	564	1.00
$Ru_{1.0}$-PLL	43	0.17	206	0.24	680	0.59	457	1.12
$Ru_{1.6}$-PLL	67	0.21	271	0.24	704	0.55	466	1.12
$Ru_{2.6}$-PLL	60	0.23	248	0.25	670	0.52	424	1.04
$Ru_{2.2}$-PLL	105	0.28	478	0.31	749	0.41	484	0.98
$Ru_{2.1}$-PLL	78	0.41	278	0.34	742	0.26	316	1.00

Table A.4f. Pre-exponential factors and decay times obtained from the fit of the fluorescence decays of the Ru-PLL samples in 0.01M NaCl aqueous solution at pH 3 with Equation 2.21.

Sample	τ_1	a_1	τ_2	a_2	τ_3	a_3	$\langle\tau\rangle_N$	χ^2
$Ru_{2.0}$-PLL	43	0.16	307	0.29	554	0.55	400	0.94
$Ru_{1.0}$-PLL	36	0.25	296	0.37	559	0.38	330	1.17
$Ru_{1.6}$-PLL	45	0.20	238	0.33	485	0.50	330	1.12
$Ru_{2.6}$-PLL	37	0.19	317	0.28	592	0.52	403	1.00
$Ru_{2.2}$-PLL	29	0.25	203	0.19	545	0.56	351	0.99
$Ru_{2.1}$-PLL	35	0.42	198	0.23	554	0.35	254	1.03

Table A.5a. FBM parameters retrieved by using the Equation 2.22 for the analysis of the fluorescence decays of the Ru-PLL-Q samples in 0.01M NaCl aqueous solution at pH 3.

Sample	$\langle n \rangle$	f_{diff}	f_{free}	$k_{blob}(10^6\ s^{-1})$	$k_{exch}(10^6\ s^{-1})$	N_{blob}	χ^2
$Ru_{1.0}$-PLL-$Q_{7.1}$	1.48	0.62	0.37	8.2	1.1	15.23	1.10
$Ru_{1.6}$-PLL-$Q_{8.4}$	1.54	0.67	0.32	10.7	1.2	13.92	0.98
$Ru_{2.6}$-PLL-$Q_{11.0}$	1.67	0.68	0.32	12.1	3.8	11.05	1.18
$Ru_{2.2}$-PLL-$Q_{11.5}$	2.00	0.64	0.35	9.1	1.5	12.13	1.04
$Ru_{2.1}$-PLL-$Q_{12.1}$	1.30	0.73	0.27	11.9	1.5	8.54	1.09

Table A.5b. FBM parameters retrieved by using the Equation 2.22 for the analysis of the fluorescence decays of the Ru-PLL-Q samples in 0.01M NaCl aqueous solution at pH 5.

Sample	$\langle n \rangle$	f_{diff}	f_{free}	$k_{blob}(10^6\ s^{-1})$	$k_{exch}(10^6\ s^{-1})$	N_{blob}	χ^2
$Ru_{1.2}$-PLL-$Q_{5.9}$	1.06	0.58	0.41	11.8	1.8	12.97	1.07
$Ru_{1.0}$-PLL-$Q_{7.1}$	0.97	0.72	0.27	12	1.5	11.64	0.95
$Ru_{1.6}$-PLL-$Q_{8.4}$	0.83	0.94	0.06	9.2	1.1	10.25	1.11
$Ru_{2.6}$-PLL-$Q_{11.0}$	1.15	0.82	0.17	8.7	1.3	9.24	1.08
$Ru_{2.2}$-PLL-$Q_{11.5}$	1.00	0.77	0.23	10.3	1.3	7.30	1.04
$Ru_{2.1}$-PLL-$Q_{12.1}$	1.10	0.78	0.21	9.8	1.3	7.71	1.12

Table A.5c. FBM parameters retrieved by using the Equation 2.22 for the analysis of the fluorescence decays of the Ru-PLL-Q samples in 0.01M NaCl aqueous solution at pH 7.

Sample	<*n*>	f_{diff}	f_{free}	$k_{blob}(10^6\ s^{-1})$	$k_{exch}(10^6\ s^{-1})$	N_{blob}	χ^2
$Ru_{1.2}$-PLL-$Q_{5.9}$	0.87	0.65	0.34	8.7	1.1	11.95	1.10
$Ru_{1.0}$-PLL-$Q_{7.1}$	0.71	0.81	0.18	9.1	1.5	9.56	1.12
$Ru_{1.6}$-PLL-$Q_{8.4}$	0.98	0.77	0.22	9.4	1.9	10.26	1.08
$Ru_{2.6}$-PLL-$Q_{11.0}$	1.08	0.85	0.14	7.8	2.4	8.99	1.06
$Ru_{2.2}$-PLL-$Q_{11.5}$	1.02	0.74	0.25	11.2	1.8	7.17	1.12
$Ru_{2.1}$-PLL-$Q_{12.1}$	0.89	0.80	0.19	11.3	2.0	6.42	1.05

Table A.5d. FBM parameters retrieved by using the Equation 2.22 for the analysis of the fluorescence decays of the Ru-PLL-Q samples in 0.01M NaCl aqueous solution at pH 9.

Sample	<*n*>	f_{diff}	f_{free}	$k_{blob}(10^6\ s^{-1})$	$k_{exch}(10^6\ s^{-1})$	N_{blob}	χ^2
$Ru_{1.2}$-PLL-$Q_{5.9}$	0.80	0.72	0.27	7.9	1.3	12.18	1.06
$Ru_{1.0}$-PLL-$Q_{7.1}$	0.79	0.85	0.14	8.9	2.8	11.44	1.02
$Ru_{1.6}$-PLL-$Q_{8.4}$	1.23	0.79	0.20	6.4	2.0	13.36	1.11
$Ru_{2.6}$-PLL-$Q_{11.0}$	1.26	0.85	0.14	5.9	1.7	10.50	1.17
$Ru_{2.2}$-PLL-$Q_{11.5}$	1.17	0.90	0.09	7.2	2.2	10.05	1.1
$Ru_{2.1}$-PLL-$Q_{12.1}$	1.15	0.79	0.20	7.4	2.2	8.20	1.03

Table A.5e. FBM parameters retrieved by using the Equation 2.22 for the analysis of the fluorescence decays of the Ru-PLL-Q samples in 0.01M NaCl aqueous solution at pH 11.

Sample	<*n*>	f_{diff}	f_{free}	$k_{blob}(10^6\ s^{-1})$	$k_{exch}(10^6\ s^{-1})$	N_{blob}	χ^2
$Ru_{1.2}$-PLL-$Q_{5.9}$	0.99	0.88	0.11	10.8	3.1	14.30	1.10
$Ru_{1.0}$-PLL-$Q_{7.1}$	1.27	0.96	0.04	4.5	4.5	20.15	1.11
$Ru_{1.6}$-PLL-$Q_{8.4}$	0.99	0.88	0.11	10.1	10.1	11.88	1.16
$Ru_{2.6}$-PLL-$Q_{11.0}$	1.01	0.80	0.19	7.5	1.6	7.93	1.16
$Ru_{2.2}$-PLL-$Q_{11.5}$	1.65	0.80	0.19	10.2	1.8	13.73	1.19
$Ru_{2.1}$-PLL-$Q_{12.1}$	0.90	0.86	0.13	8.9	1.2	6.97	1.01

Table A.5f. FBM parameters retrieved by using the Equation 2.22 for the analysis of the fluorescence decays of the Ru-PLL-Q samples in 0.01M NaCl aqueous solution at pH 13.

Sample	<*n*>	f_{diff}	f_{free}	$k_{blob}(10^6\ s^{-1})$	$k_{exch}(10^6\ s^{-1})$	N_{blob}	χ^2
$Ru_{1.2}$-PLL-$Q_{5.9}$	1.38	0.77	0.22	12.6	2.1	15.48	1.15
$Ru_{1.0}$-PLL-$Q_{7.1}$	1.66	0.68	0.31	9.3	9.3	18.66	1.06
$Ru_{1.6}$-PLL-$Q_{8.4}$	1.38	0.81	0.18	11.8	2.7	15.15	1.14
$Ru_{2.6}$-PLL-$Q_{11.0}$	0.89	0.89	0.10	11.1	2.6	7.84	1.12
$Ru_{2.2}$-PLL-$Q_{11.5}$	1.25	0.89	0.10	13.4	1.6	10.57	1.02
$Ru_{2.1}$-PLL-$Q_{12.1}$	0.62	0.85	0.14	34.7	3.7	4.67	0.96